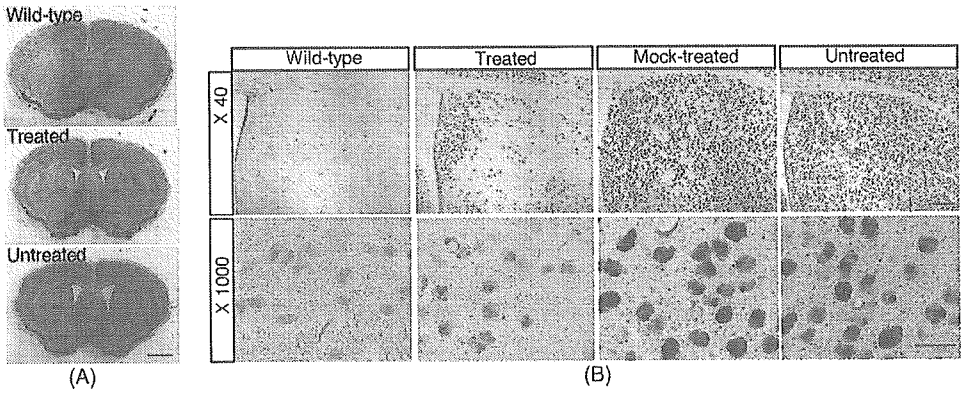

Fig. 5. Brain atrophy was inhibited and huntingtin-immunoreactive intranuclear inclusions were significantly reduced in siRNA-HDExon1-treated R6/2 mice. (A) Effect of siRNA-HDExon1 on ventricular enlargement and striatal atrophy. Upper panel, wild-type; middle panel, siRNA-treated; lower panel, untreated. Scale bar: 100 μm. (B) Brains from 8-week-old mice were immunostained with an antibody against mutant huntingtin (MAB5374), which recognizes the N-terminal portion of this protein. Neuronal intranuclear inclusions of mutant huntingtin were abundant in the striatum of mock-treated and untreated R6/2 mice. Compared with those mice, siRNA-HDExon1-treated R6/2 mice showed a decrease in number of cells with intranuclear inclusions in the striatum. Scale bars: 200 μm for upper panels (magnification ×40) and 30 μm for lower panels (magnification ×1000).

2 mice of the same age (8 weeks; Fig. 5(B)). However, these effects were locally confirmed in the striatum especially at the injection site, but not in remote areas of the ventricle such as the cortex. We also noticed that, in siRNA-treated mice, NII-positive neurons were not evenly distributed in different areas of the striatum, perhaps a consequence of the uneven diffusion of the solution containing the siRNA-transfection complex following the initial injection into the brain (Fig. 5(B)).

4. Discussion

Using cultured cells or HD model mice, there are numerous experimental approaches to address potential therapeutic strategies for HD based on different principles (Chen et al., 2000; Ferrante et al., 2003; Tanaka et al., 2004). However, since the expression of mutant htt in neurons is a crucial and fundamental event in HD in terms of "gain-of-function" theory (Kennedy et al., 2003; Schaffar et al., 2004), the most plausible strategy to combat HD would be to suppress mutant htt expression specifically in the brain. HD transgenic mice, R6/2, develop a neurodegenerative syndrome that closely models the human disease. Here we show that siRNA treatment of these mice from an early age helps to prevent the loss of body weight, extend longevity and delay the onset of motor dysfunction. Besides these beneficial effects, siRNAs induce down-regulation of transgenic htt expression and decrease the density and number of NII in striatal neurons. This work may represent the first successful use of siRNA in HD mouse model R6/2.

Surprisingly, a beneficial effect of siRNA could be attained after only one intraventricular injection, just after birth. Moreover, the effect was unexpectedly long lasting. The silencing effect of siRNA in replicating cells usually reaches a maximum around the fourth day and lasts no longer than 1 week (Novina et al., 2002; Tuschl, 2002). Although there is little evidence for the long-lasting effect of siRNA in post-mitotic cells such as neurons or muscle cells, the effect of siRNA has been sustained for at least 15 days in non-dividing macrophages (Song et al., 2003). It is, therefore, quite striking that the effect of the siRNA, siRNA-HDExon1, was apparently sustained so as to prolong the lifespan of R6/2 (Fig. 2(B)). The sustained siRNA effect in the brain could have been due to a reduced degradation rate of siRNA in post-mitotic cells via an unknown mechanism. However, another possibility is that the single application of siRNA-HDExon1 could have had a long-lasting suppressive effect on protein synthesis.

One of the distinct characteristics of HD is that its development is progressive, with onset occurring in middle age in human patients. Now that a pre-symptomatic genetic test is available, pre-clinical treatment may be feasible. An important point is the age at which a pre-symptomatic HD patient should begin preclinical treatment. Our work now shows that the application of siRNA directly into the brain of newborn mice (P2) results in significant improvement in both the symptoms and motor function of these HD model animals. We therefore postulate that the use of siRNA soon after birth—before NII formation/accumulation begins—may suppress mutant htt expression and thus block disease development.

Even though our results are very encouraging, there are still many experimental details to be investigated prior to the use of this technology in the clinic. We must refine our ability to efficiently and stably produce and deliver sufficient amounts of siRNA to the proper target tissues. Researchers have recently used plasmid and viral vectors to transcribe short-hairpin RNAs (shRNA), both in vitro and in vivo. Viral vectors expressing an shRNA directed against the mutant *SCA1* gene functioned similarly to

siRNA to rescue the clinical symptoms and pathology of a mouse model of spinocerebellar ataxia 1, another disease related to expanded CAG repeats (Xia et al., 2004). During the editorial process of this paper, Harper et al. (2005) have shown that RNA interference induced by viral vectors improves motor and neuropathological abnormalities in another HD mouse model which is HD transgenic containing 82 CAG repeats and with a milder HD-like phenotype compared to R6/2 used here (Harper et al., 2005). Although vector-based shRNA-mediated RNAi activates interferon response in vitro, whereas siRNA does not induce the type 1 interferon response (Bridge et al., 2003), this system achieves more stable inhibition of gene expression compared with transient delivery of chemically synthesized siRNA. We have also generated such vectors against the htt gene and proved them to be effective and specific in cell culture models. Their effects on R6/2 are now being tested.

Compared with adenoviral vectors (10^{10} pfu/ml), gene expression following cationic DNA-liposome complex transfection is approximately 20-fold lower, but without biochemical, hematological and histopathological abnormalities (Stephan et al., 1996). Thus, we conclude that a delivery system with little or no toxicity, but with high efficiency and selectivity, is required before clinical trials. Although there were some minor variations among individual mice, the distribution pattern of the dye injected with the DNA-liposome complex was consistent and reproducible, and our results do not reflect non-specific technical aspects of the injection procedure.

Wild-type htt is essential for embryogenesis since an htt gene knockout in mice causes early embryonic lethality (Duyao et al., 1995; Nasir et al., 1995; Zeitlin et al., 1995). Conditional knockout of the mouse htt gene after postnatal day 5 results in progressive neurodegeneration in the adult mouse (Dragatsis et al., 2000). It would therefore be ideal to reduce the expression of the mutant htt gene independently of the wild-type gene. However, it has been practically impossible to design an siRNA sequence that is selective for mutant htt. In this study, there are three base pair differences in the siRNA-HDExon1 targeted region of mouse htt, and siRNA may not suppress mouse homologous huntingtin expression. We currently have no data on whether siRNA-HDExon1 reduced expression of mouse endogenous htt in vivo, except that we did not identify any affected phenotypes in siRNA-treated wild-type mouse.

We have shown that siRNA can improve the clinical and pathological abnormalities manifested by an animal model of HD. We obtained our results using a mouse model carrying a mutant transgene encoding exon 1 of the human htt gene. Therefore, the application of our method is limited at present. However, even if wild-type htt is indeed essential for neuronal survival, it will certainly be possible to define an appropriate "therapeutic window" for partial suppression of the htt gene, thereby providing a new treatment strategy for HD.

Acknowledgements

We thank K. Sakurai (The Jikei University School of Medicine, Japan), H. Ohashi, H. Kikuchi, M. Sekiguchi and H. Hohjoh for technical assistance and A. Takahashi for animal care. This work was approved by the Ethics Committee of the Institute and supported by a grant, Solution Oriented Research for Science and Technology (SORST), from the Japan Science and Technology Agency (JST) and Grants-in-Aid for Scientific Research from the Ministry of Health, Labour and Welfare of Japan.

References

Boado, R.J., Kazantsev, A., Apostol, B.L., Thompson, L.M., Pardridge, W.M., 2000. Antisense-mediated down-regulation of the human huntingtin gene. J. Pharmacol. Exp. Ther. 295, 239–243.

Bridge, A.J., Pebernard, S., Ducraux, A., Nicoulaz, A.L., Iggo, R., 2003. Induction of an interferon response by RNAi vectors in mammalian cells. Nat. Genet. 34, 263–264.

Busch, A., Engemann, S., Lurz, R., Okazawa, H., Lehrach, H., Wanker, E.E., 2003. Mutant huntingtin promotes the fibrillogenesis of wild-type huntingtin: a potential mechanism for loss of huntingtin function in Huntington's disease. J. Biol. Chem. 278, 41452–41461.

Chen, M., Ona, V.O., Li, M., Ferrante, R.J., Fink, K.B., Zhu, S., Bian, J., Guo, L., Farrell, L.A., Hersch, S.M., Hobbs, W., Vonsattel, J.P., Cha, J.H., Friedlander, R.M., 2000. Minocycline inhibits caspase-1 and caspase-3 expression and delays mortality in a transgenic mouse model of Huntington disease. Nat. Med. 6, 797–801.

DiFiglia, M., Sapp, E., Chase, K.O., Davies, S.W., Bates, G.P., Vonsattel, J.P., Aronin, N., 1997. Aggregation of huntingtin in neuronal intranuclear inclusions and dystrophic neurites in brain. Science 277, 1990–1993.

Dragatsis, I., Levine, M.S., Zeitlin, S., 2000. Inactivation of Hdh in the brain and testis results in progressive neurodegeneration and sterility in mice. Nat. Genet. 26, 300–306.

Duyao, M.P., Auerbach, A.B., Ryan, A., Persichetti, F., Barnes, G.T., McNeil, S.M., Ge, P., Vonsattel, J.P., Gusella, J.F., Joyner, A.L., 1995. Inactivation of the mouse Huntington's disease gene homolog Hdh. Science 269, 407–410.

Ferrante, R.J., Kubilus, J.K., Lee, J., Ryu, H., Beesen, A., Zucker, B., Smith, K., Kowall, N.W., Ratan, R.R., Luthi-Carter, R., Hersch, S.M., 2003. Histone deacetylase inhibition by sodium butyrate chemotherapy ameliorates the neurodegenerative phenotype in Huntington's disease mice. J. Neurosci. 23, 9418–9427.

Gines, S., Seong, I.S., Fossale, E., Ivanova, E., Trettel, F., Gusella, J.F., Wheeler, V.C., Persichetti, F., MacDonald, M.E., 2003. Specific progressive cAMP reduction implicates energy deficit in presymptomatic Huntington's disease knock-in mice. Hum. Mol. Genet. 12, 497–508.

Gusella, J.F., MacDonald, M.E., 2000. Molecular genetics: unmasking polyglutamine triggers in neurodegenerative disease. Nat. Rev. Neurosci. 1, 109–115.

Haque, N.S., Borghesani, P., Isacson, O., 1997. Therapeutic strategies for Huntington's disease based on a molecular understanding of the disorder. Mol. Med. Today 3, 175–183.

Harper, S.Q., Staber, P.D., He, X., Eliason, S.L., Martins, I.H., Mao, Q., Yang, L., Kotin, R.M., Paulson, H.L., Davidson, B.L., 2005. From the Cover: RNA interference improves motor and neuropathological abnormalities in a Huntington's disease mouse model. Proc. Natl. Acad. Sci. U.S.A. 102, 5820–5825.

Hazeki, N., Tsukamoto, T., Yazawa, I., Koyama, M., Hattori, S., Someki, I., Iwatsubo, T., Nakamura, K., Goto, J., Kanazawa, I., 2002. Ultrastructure

of nuclear aggregates formed by expressing an expanded polyglutamine. Biochem. Biophys. Res. Commun. 294, 429–440.

Kaytor, M.D., Wilkinson, K.D., Warren, S.T., 2004. Modulating huntingtin half-life alters polyglutamine-dependent aggregate formation and cell toxicity. J. Neurochem. 89, 962–973.

Kennedy, L., Evans, E., Chen, C.M., Craven, L., Detloff, P.J., Ennis, M., Shelbourne, P.F., 2003. Dramatic tissue-specific mutation length increases are an early molecular event in Huntington disease pathogenesis. Hum. Mol. Genet. 12, 3359–3367.

Liu, W., Goto, J., Wang, Y., Murata, M., Wada, K., Kanazawa, I., 2003. Specific inhibition of Huntington's disease gene expression by siRNAs in cultured cells. Proc. Jpn. Acad. 79 (Ser. B), 293–298.

Mangiarini, L., Sathasivam, K., Mahal, A., Mott, R., Seller, M., Bates, G.P., 1997. Instability of highly expanded CAG repeats in mice transgenic for the Huntington's disease mutation. Nat. Genet. 15, 197–200.

Mangiarini, L., Sathasivam, K., Seller, M., Cozens, B., Harper, A., Hetherington, C., Lawton, M., Trottier, Y., Lehrach, H., Davies, S.W., Bates, G.P., 1996. Exon 1 of the HD gene with an expanded CAG repeat is sufficient to cause a progressive neurological phenotype in transgenic mice. Cell 87, 493–506.

Menalled, L.B., Chesselet, M.F., 2002. Mouse models of Huntington's disease. Trends Pharmacol. Sci. 23, 32–39.

Nasir, J., Floresco, S.B., O'Kusky, J.R., Diewert, V.M., Richman, J.M., Zeisler, J., Borowski, A., Marth, J.D., Phillips, A.G., Hayden, M.R., 1995. Targeted disruption of the Huntington's disease gene results in embryonic lethality and behavioral and morphological changes in heterozygotes. Cell 81, 811–823.

Nellemann, C., Abell, K., Norremolle, A., Lokkegaard, T., Naver, B., Ropke, C., Rygaard, J., Sorensen, S.A., Hasholt, L., 2000. Inhibition of Huntington synthesis by antisense oligodeoxynucleotides. Mol. Cell Neurosci. 16, 313–323.

Novina, C.D., Murray, M.F., Dykxhoorn, D.M., Beresford, P.J., Riess, J., Lee, S.K., Collman, R.G., Lieberman, J., Shankar, P., Sharp, P.A., 2002. siRNA-directed inhibition of HIV-1 infection. Nat. Med. 8, 681–686.

Obrietan, K., Hoyt, K.R., 2004. CRE-mediated transcription is increased in Huntington's disease transgenic mice. J. Neurosci. 24, 791–796.

Sakurai, K., Iizuka, S., Shen, J.S., Meng, X.L., Mori, T., Umezawa, A., Ohashi, T., Eto, Y., 2004. Brain transplantation of genetically modified bone marrow stromal cells corrects CNS pathology and cognitive function in MPS VII mice. Gene Ther. 11, 1475–1481.

Schaffar, G., Breuer, P., Boteva, R., Behrends, C., Tzvetkov, N., Strippel, N., Sakahira, H., Siegers, K., Hayer-Hartl, M., Hartl, F.U., 2004. Cellular toxicity of polyglutamine expansion proteins: mechanism of transcription factor deactivation. Mol. Cell. 15, 95–105.

Shen, J.S., Meng, X.L., Ohashi, T., Eto, Y., 2002. Adenovirus-mediated prenatal gene transfer to murine central nervous system. Gene Ther. 9, 819–823.

Shen, J.S., Watabe, K., Ohashi, T., Eto, Y., 2001. Intraventricular administration of recombinant adenovirus to neonatal twitcher mouse leads to clinicopathological improvements. Gene Ther. 8, 1081–1087.

Song, E., Lee, S.K., Dykxhoorn, D.M., Novina, C., Zhang, D., Crawford, K., Cerny, J., Sharp, P.A., Lieberman, J., Manjunath, N., Shankar, P., 2003. Sustained small interfering RNA-mediated human immunodeficiency virus type 1 inhibition in primary macrophages. J. Virol. 77, 7174–7181.

Stephan, D.J., Yang, Z.Y., San, H., Simari, R.D., Wheeler, C.J., Felgner, P.L., Gordon, D., Nabel, G.J., Nabel, E.G., 1996. A new cationic liposome DNA complex enhances the efficiency of arterial gene transfer in vivo. Hum. Gene Ther. 7, 1803–1812.

Sugars, K.L., Brown, R., Cook, L.J., Swartz, J., Rubinsztein, D.C., 2004. Decreased cAMP response element-mediated transcription: an early event in exon 1 and full-length cell models of Huntington's disease that contributes to polyglutamine pathogenesis. J. Biol. Chem. 279, 4988–4999.

Tanaka, M., Machida, Y., Niu, S., Ikeda, T., Jana, N.R., Doi, H., Kurosawa, M., Nekooki, M., Nukina, N., 2004. Trehalose alleviates polyglutamine-mediated pathology in a mouse model of Huntington disease. Nat. Med. 10, 148–154.

Trushina, E., Heldebrant, M.P., Perez-Terzic, C.M., Bortolon, R., Kovtun, I.V., Badger 2nd, J.D., Terzic, A., Estevez, A., Windebank, A.J., Dyer, R.B., Yao, J., McMurray, C.T., 2003. Microtubule destabilization and nuclear entry are sequential steps leading to toxicity in Huntington's disease. Proc. Natl. Acad. Sci. U.S.A. 100, 12171–12176.

Tuschl, T., 2002. Expanding small RNA interference. Nat. Biotechnol. 20, 446–448.

Xia, H., Mao, Q., Eliason, S.L., Harper, S.Q., Martins, I.H., Orr, H.T., Paulson, H.L., Yang, L., Kotin, R.M., Davidson, B.L., 2004. RNAi suppresses polyglutamine-induced neurodegeneration in a model of spinocerebellar ataxia. Nat. Med. 10, 816–820.

Yamamoto, A., Lucas, J.J., Hen, R., 2000. Reversal of neuropathology and motor dysfunction in a conditional model of Huntington's disease. Cell 101, 57–66.

Yen, L., Strittmatter, S.M., Kalb, R.G., 1999. Sequence-specific cleavage of Huntingtin mRNA by catalytic DNA. Ann. Neurol. 46, 366–373.

Zeitlin, S., Liu, J.P., Chapman, D.L., Papaioannou, V.E., Efstratiadis, A., 1995. Increased apoptosis and early embryonic lethality in mice nullizygous for the Huntington's disease gene homologue. Nat. Genet. 11, 155–163.

Overexpression of Ubiquitin Carboxyl-Terminal Hydrolase L1 Arrests Spermatogenesis in Transgenic Mice

YU-LAI WANG,[1] WANZHAO LIU,[1] YING-JIE SUN,[2] JUNGKEE KWON,[1,3] RIEKO SETSUIE,[1,4] HITOSHI OSAKA,[1] MAMI NODA,[4] SHUNSUKE AOKI,[1] YASUHIRO YOSHIKAWA,[3] AND KEIJI WADA[1]*

[1]*Department of Degenerative Neurological Diseases, National Institute of Neuroscience, NCNP, Kodaira, Tokyo, Japan*
[2]*Department of Anatomy and Structural Science, Yamagata University School of Medicine, Yamagata, Japan*
[3]*Department of Biomedical Science, Graduate School of Agricultural and Life Sciences, University of Tokyo, Bunkyo-ku, Tokyo, Japan*
[4]*Laboratory of Pathophysiology, Graduate School of Pharmaceutical Sciences, Kyushu University, Higashi-ku, Fukuoka, Japan*

ABSTRACT Ubiquitin carboxyl-terminal hydrolase 1 (UCH-L1) can be detected in mouse testicular germ cells, mainly spermatogonia and somatic Sertoli cells, but its physiological role is unknown. We show that transgenic (Tg) mice overexpressing *EF1α* promoter-driven UCH-L1 in the testis are sterile due to a block during spermatogenesis at an early stage (pachytene) of meiosis. Interestingly, almost all spermatogonia and Sertoli cells expressing excess UCH-L1, but little PCNA (proliferating cell nuclear antigen), showed no morphological signs of apoptosis or TUNEL-positive staining. Rather, germ cell apoptosis was mainly detected in primary spermatocytes having weak or negative UCH-L1 expression but strong PCNA expression. These data suggest that overexpression of UCH-L1 affects spermatogenesis during meiosis and, in particular, induces apoptosis in primary spermatocytes. In addition to results of caspases-3 upregulation and Bcl-2 downregulation, excess UCH-L1 influenced the distribution of PCNA, suggesting a specific role for UCH-L1 in the processes of mitotic proliferation and differentiation of spermatogonial stem cells during spermatogenesis. *Mol. Reprod. Dev. 73: 40–49, 2006.* © 2005 Wiley-Liss, Inc.

Key Words: UCH-L1; transgenic mouse; spermatogenesis; testis; apoptosis

INTRODUCTION

Mammalian spermatogenesis is a complex process of cellular differentiation. Spermatogonia serve as the self-renewing stem cells for spermatogenesis and undergo mitotic divisions that yield primary spermatocytes (Matzuk and Lamb, 2002). In addition to germ cells, somatic Sertoli cells also are a major cell population in the testis, comprising the seminiferous tubule epithelium that nurtures germ cells (Imai et al., 2004).

Components of the ubiquitin system appear to be involved in different steps and processes during spermatogenesis (Baarends et al., 2000; Sutovsky, 2003). Ubiquitin is a highly evolutionarily conserved 76-residue polypeptide that plays a critical role in many cellular processes, including the cell cycle, cell proliferation, development, apoptosis, signal transduction, and membrane protein internalization (Williams et al., 2002). Ubiquitin appears to be expressed in mammalian testes/ovaries and embryos at all developmental steps, and its level is modulated by ubiquitynating and deubiquitynating enzymes. However, the details of the involvement of these enzymes in ubiquitin-dependent proteolysis during gametogenesis and fertilization remain uncertain. Several deubiquitynating enzymes were recently reported (Wilkinson, 2000; Wing, 2003) and have been classified as either ubiquitin carboxyl-terminal hydrolases (UCHs) or ubiquitin-specific processing proteases. UCHs liberate free ubiquitin by cleaving ubiquitin-containing covalent complexes, namely ubiquitylated small ribosomal proteins (L40, S27a) or tandemly conjugated polyubiquitin (e.g., UbB, UbC) (Wilkinson, 2000). UCHs can also hydrolyze bonds between ubiquitin and small adducts or unfolded polypeptides in vitro. Thus, UCHs are thought to serve dual functions: to salvage ubiquitin that has been trapped by reactions with low-molecular weight thiols/amines and to process polyubiquitin or ubiquitylated proteins.

In mice, there are at least four closely related low-molecular weight UCH family members, UCH-L1 and UCH-L3–5 (Kurihara et al., 2001; Osawa et al., 2001). The distribution and function of UCH-L4 and UCH-L5 are not clear. UCH-L3, however, is expressed ubiquitously, whereas UCH-L1 is selectively expressed in the testis/ovary and brain. Moreover, UCH-L1 is highly

Grant sponsor: Ministry of Health, Labour, and Welfare of Japan.

*Correspondence to: Dr. Keiji Wada, Department of Degenerative Neurological Diseases, National Institute of Neuroscience, NCNP, Kodaira, Tokyo 187-8502, Japan. E-mail: wada@ncnp.go.jp

Received 4 May 2005; Accepted 30 June 2005
Published online 21 September 2005 in Wiley InterScience (www.interscience.wiley.com).
DOI 10.1002/mrd.20364

expressed in mouse spermatogonia and somatic Sertoli cells but not in post meiotic germ cells (Kwon et al., 2004a). By contrast, UCH-L3 is detected mainly in spermatocytes and round spermatids (Kwon et al., 2004a). These two isozymes are considered to play important roles in the labeling/targeting of abnormal proteins for degradation via the ubiquitin-proteasome system (Wilkinson, 2000).

The gracile axonal dystrophy (*gad*) mouse is an autosomal recessive spontaneous mutant carrying an intragenic deletion of the gene encoding UCH-L1 (*Uchl1*). *gad* mice do not express UCH-L1 and thus are comparable to a *Uchl1* null mutant (Yamazaki et al., 1988; Saigoh et al., 1999). We recently showed that *gad* mice are resistant to the germ cell apoptosis during the first round of spermatogenesis (Kwon et al., 2005) and are also resistant to cryptorchid-induced testicular germ cell apoptosis (Kwon et al., 2004b). The expression of the apoptotic proteins p53, Bax, and caspases-3 was significantly lower in the immature testes, and the expression of both antiapoptotic and prosurvival proteins such as Bcl-2, Bcl-xL, XIAP, pCREB, and BDNF was significantly higher in *gad* mice following experimental cryptorchidism (Kwon et al., 2004b). These data prompted our hypothesis that UCH-L1 may be an important regulator of apoptosis during spermatogenesis. Experiments toward this end may provide additional evidence that UCH-L1 regulates spermatogenesis.

Our present report presents the characterization of the male sterility phenotype and the quantitation of apoptotic spermatocytes in *Uchl1* transgenic (Tg) mice. Constitutive expression of UCH-L1 in the testis results in a blockade of spermatogenesis at the pachytene stage of spermatocytes due to an increase in the number of apoptotic spermatocytes. These results indicate that excess UCH-L1 affects spermatogenesis during meiosis and, in particular, induces apoptosis in primary spermatocytes.

MATERIALS AND METHODS

Animals

We have previously described the Tg *Uchl1* mice carrying a 0.7-kb FLAG-tagged mouse *Uchl1* cDNA with the human translation elongation factor-1α (*EF-1α*) promoter (Osaka et al., 2003). Tg mice were identified by PCR analysis of tail DNA using specific primers (forward: ex6F, 5′-ATCCAGGCGGCCCATGACCTC-3′; reverse: ex9R, 5′-AGCTGCTTTGCAGAGAGCCA-3′). The *gad* mouse is an autosomal recessive mutant that was obtained by crossing CBA and RFM mice (Saigoh et al., 1999). All strains were maintained at our institute. To corroborate fertility disturbances in UCH-L1 Tg mice, a subset of the mice was continuously mated with wild-type C57BL/6J mice. The mating of two heterozygous Tg males with non-Tg females did not yield offspring until the age of 6 months despite grossly normal appearance. This was also the case for the mating of four heterozygous Tg females with non-Tg males. Their non-Tg littermates sired offspring normally. Finally, all six Tg mice were infertile, but they did not exhibit any apparent neurological phenotype during adulthood. Controls included nontransgenic (non-Tg) littermates and UCH-L1-deficient *gad* mice (Saigoh et al., 1999). Mice were sacrificed by cervical dislocation before tissue collection. Animal care and handling were in accordance with institutional regulations for animal care and were approved by the Animal Investigation Committee of the National Institute of Neuroscience, National Center of Neurology and Psychiatry of Japan.

mRNA Isolation, and Exogenous *Uchl1* Expression Measured by Quantitative Real-Time RT-PCR

Total RNA from testes was isolated using the Trizol reagent (Gibco BRL Life Technologies, Bethesda, MD) and purified following the manufacturer's instructions. Real-time quantitative RT-PCR primer pairs flanking introns were used to specifically amplify transgene products, and their sequences were: forward, 5′-ATTT-CAGGTGTCGTGAGGAA-3′; and reverse, 5′-CCCAC-GTGGGAGACCTGATA-3′. Real-time quantitative PCR products, from 0.25–2.5 ng of reverse-transcribed cDNA samples, were detected using an ABI Prism, 7700 system (Applied Biosystems) as described previously (Aoki et al., 2002). β-Actin and GAPDH were used as endogenous controls. Results are expressed as the ratio of the mRNA level of the transgene to that of β-actin or GAPDH. As an external standard for quantitative analysis, the cDNA of the 3′-noncoding region of mouse *Uchl1* cDNA (covering the RT-PCR primers) was cloned and inserted into a pcDNA3 vector, purified, precisely quantified, and serially diluted 10-fold to 10 copies/μl. Standard curves were determined using linear regression analysis of the Ct values relative to plasmid copy numbers. In each real-time quantitative PCR assay, a 10-fold serially diluted cDNA template series was added to construct a standard curve for copy number. Each sample was analyzed in triplicate, and copy numbers were determined from each corresponding standard curve by the ratio of Tg *UCH-L1* to mouse *Uchl1*.

Histological Observations, Immunohistochemistry, and Immunofluorescence

Morphological studies were performed on six male controls and two male Tg mice (Tg21 and Tg22, both 6 months old). The two control groups consisted of three non-Tg wild-type C57BL/6J mice, 6 months old, littermates, and three *gad* mice, age 4 months. Testes were fixed in 4% paraformaldehyde for 24 hr and embedded in paraffin. Serial 5-μm sections were used for histology after hematoxylin–eosin staining as well as for immunohistochemistry and the TUNEL assay. Primary monoclonal or polyclonal antibodies against the following proteins were used at the final dilutions indicated: UCH-L1 (RA95101, Ultraclone, Lucigen, Middleton, WI, 1:2,000), FLAG (FM2, Sigma, St. Louis, MO, 1:500), PCNA (PC10, Santa Cruz Biotechnology, Santa Cruz, CA, 1:200), PCNA (Clone 24, BD Transduction

Laboratory, Lexington, KY, 1:2,000), vimentin (Zymed, 1:100), and ubiquitin (Dako, Carpenteria, CA, 1:400). For controls, the primary antibody was replaced with normal rabbit serum or was omitted (these controls always yielded negative staining). For immunofluorescence studies, secondary antibodies were anti-mouse-Cy3 or -FITC or anti-rabbit-conjugated-Cy3 or -FITC (Jackson ImmunoResearch, West Grove, PA, 1:500).

TUNEL Assay

TUNEL staining was performed according to the original protocol, with modifications (Harada et al., 2004). The number of apoptotic cells was determined by counting positively stained nuclei in 30 tubule cross-sections per testis section in each testis (Kwon et al., 2004b). For clarity and brevity, we also counted all the TUNEL-stained cells within the entire cell population of testicular tubules in each section. In addition, we also counted the apoptosis-positive tubules (i.e., tubules containing at least one apoptotic cell) in each testis.

Western Blotting

Protein lysates were prepared from mouse testes as described (Kwon et al., 2004b). Approximately 20 μg of total protein was loaded per lane on 15% SDS–PAGE gels. Primary antibodies (diluted as indicated) were used to detect the following proteins: UCH-L1 (RA95101, 1:5,000), FLAG (FM2, Sigma, 1:2,000), Bcl-2 (Cell Signaling, Beverly, MA, 1:1,000), caspase-3 (Cell Signaling, 1:400), polyubiquitin (FK2 clone, Medical & Biological Laboratory, Nagoya, Japan, 1:1,000), and monoubiquitin (U5379, Sigma, 1:1,000). Blots were further incubated with peroxidase-conjugated goat anti-mouse IgG or goat anti-rabbit IgG (1:5,000; Pierce, Rockford, IL) for 1 hr at room temperature. Immunoreactions were visualized using the SuperSignal West Dura extended duration substrate (Pierce) and analyzed with a ChemiImager (Alpha Innotech, San Leandro, CA). ChemiImager data were analyzed using AlphaEase software (Alpha Innotech) to yield the relative level of each protein.

RESULTS

Sterile Phenotype of *Uchl1* Tg Mice

We initially attempted to overexpress *Uchl1* in neurons using a Tg construct containing the *EF-1α* promoter (Mizushima and Nagata, 1990). The transgene was also strongly expressed in gonads as well as other Tg mice via the same promoter (Furuchi et al., 1996). We obtained six Tg mice having high transgene copy number, each of which most likely carried the transgene in a unique genomic location (see below). Four of these mice were females (Tg11, Tg12, Tg43, Tg81) and two were males (Tg21 and Tg22). Unexpectedly, all of these Tgs were sterile. Thus, it was not possible to maintain Tg lines during the course of these experiments. However, in addition to the sterile phenotype, the six independent Tg mice showed a similar pattern of *Uchl1* transgene expression and common pathological defects, the latter being limited to the testes or ovaries. The Tg loci were generated by random integration rather than by site-specific recombination, and thus the animals produced by our Tg procedure usually had more than one transgene integrated at each chromosomal site (Kroll and Amaya, 1996). Therefore, in each of the six Tg mice, the transgene most likely integrated into a different genomic site, raising the possibility of different position-dependent effects. Our data showed that we obtained multiple animals with similar patterns or levels of *Uchl1* transgene expression and with common pathological defects, suggesting the phenotypes reflect position-independent expression (i.e., independent of the position of transgene insertion). Thus, these Tg mice had similar infertile phenotypes that may be attributed to the overproduction of UCH-L1. Numerous gene inactivation studies have identified gene products involved in male fertility, but in most cases female reproduction was unaffected or weak damaged (Yuan et al., 2000). However, both male and female *Uchl1* Tg mice were infertile, although there were clear differences in germinal cell maturation, suggesting that UCH-L1 is required for both spermatogenesis and oogenesis. Therefore, six independent Tg founders, notably two males (Tg21 and Tg22), were analyzed in our present study.

The mating of two heterozygous Tg males with non-Tg females did not yield offspring until the age of 6 months, despite grossly normal appearance. This was also the case for the mating of four heterozygous Tg females with non-Tg males. Their non-Tg littermates sired offspring normally. At autopsy, the testes of both Tg21 and Tg22 appeared grossly smaller than those of non-Tg mice. The testes weight of Tg21 (77 mg) and Tg22 (70 mg) was only 42% and 38%, respectively, relative to non-Tg males (183 ± 16 mg), demonstrating that mice overexpressing UCH-L1 display profoundly defective testis development.

Expression Levels of the *Uchl1* Transgene

We used RT-PCR and primers specific for the *Uchl1* transgene to compare transgene expression levels in the testes or ovaries of the six Tg mice. There was some variation between animals (Fig. 1A). All the Tgs expressed a similar level of endogenous *Uchl1* mRNA (Fig. 1A); quantitation of absolute Tg *Uchl1* copy numbers using real-time quantitative RT-PCR showed that all six Tgs expressed 2.9–6.8-fold more *Uchl1* transgene mRNA compared with endogenous mRNA (4.5, 3.6, 6.2, 3.7, 2.9, and 6.8 for Tg21, Tg22, Tg11, Tg12, Tg43, and Tg81, respectively). Relative UCH-L1 protein expression was similar among four of the Tgs (76.1 ± 5.2; Fig. 1B) but was somewhat higher in Tg 21 (100) and Tg81 (106.2). The average level of endogenous UCH-L1 expression in Tg mice was ~91% relative to non-Tg mice (Fig. 1B).

Immunohistochemistry of testicular sections using an antibody against FLAG revealed that exogenous UCH-L1 localized mainly in spermatogonia and Sertoli cells (Fig. 2E), similar to the localization of endogenous UCH-L1 (Fig. 2A). Endogenous UCH-L1 localized to both the cytoplasm and nucleus of spermatogonia and Sertoli

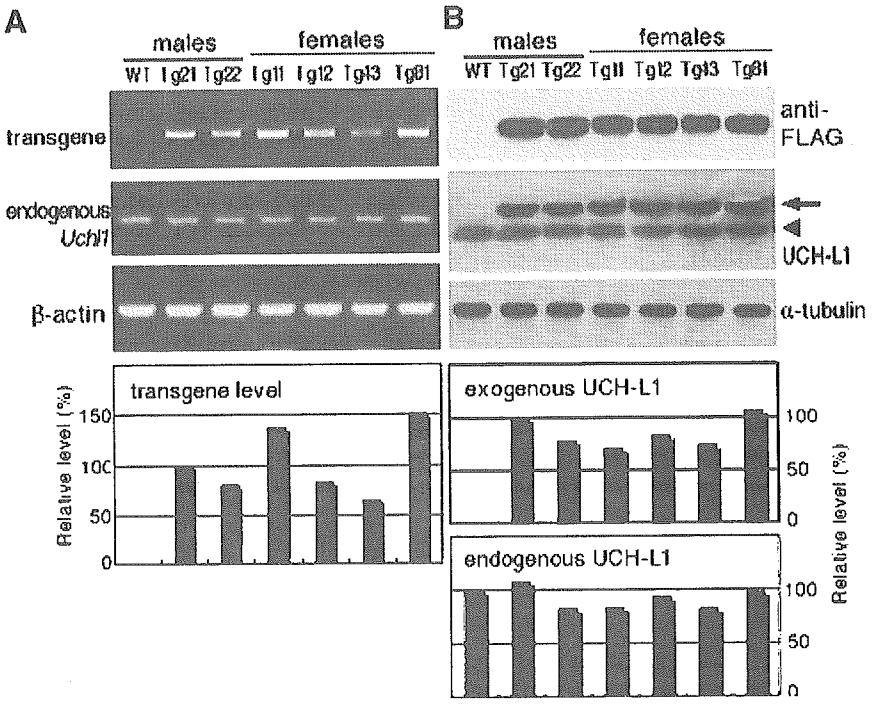

Fig. 1. Expression of transgenic ubiquitin carboxyl-terminal hydrolase 1 (UCH-L1) in the testes of Tg21 and Tg22 male mice. **A**: Transgenic *Uchl1* mRNA levels in the testes. RT-PCR showed high levels of *Uchl1* transgene mRNA in both Tg21 and Tg22 as well as in all ovaries from four female Tg mice. All Tg mice had a normal level of endogenous *Uchl1* mRNA. The relative expression level is indicated below each lane (as a percentage, scaled to β-actin in each lane). **B**: Western blot analysis of testicular or ovarian lysates. Both endogenous and exogenous UCH-L1 were detected with anti-UCH-L1, whereas exogenous UCH-L1 was specifically detected by anti-FLAG. Exogenous UCH-L1 (arrow) is slightly larger than endogenous UCH-L1 (arrowhead). WT, non-Tg wild-type.

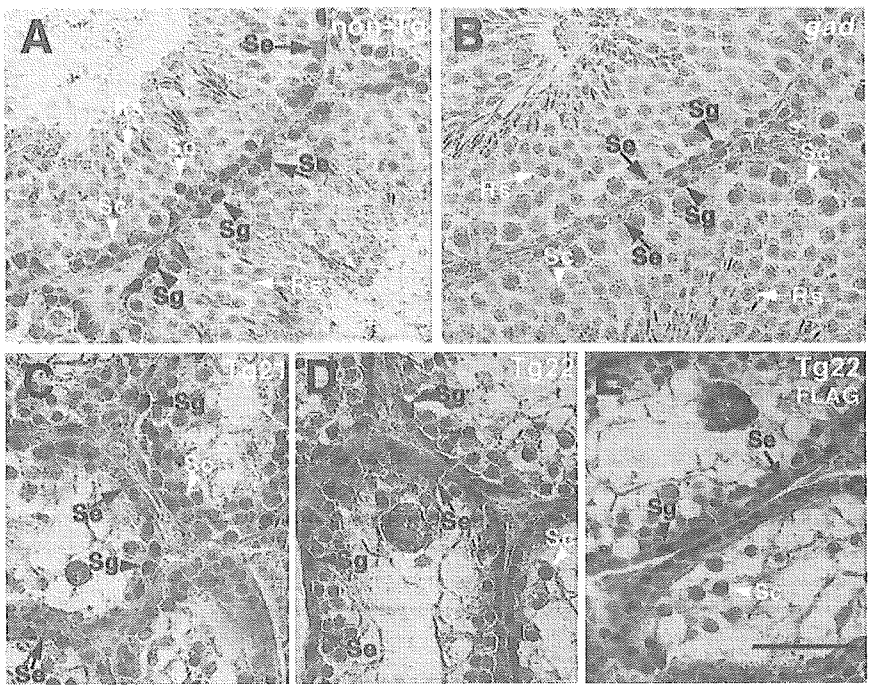

Fig. 2. Immunostaining of FLAG and UCH-L1 in *Uchl1* Tg mice shows high levels of UCH-L1 in testicular tubules. UCH-L1 immunostaining is clearly present in spermatogonia (Sg) and Sertoli cells (Se) of a non-Tg mouse (**A**) but not in a *gad* mouse (**B**). In contrast, in the testes of two Tg males, the most intense UCH-L1 immunoreactivity occurs predominantly in spermatogonia (Sg, arrowheads) and Sertoli cells (Se, arrows) but not in the primary spermatocytes (Sc, white arrowheads; **C**, Tg21; **D**, Tg22). **E**: Immunostaining of FLAG confirmed the transgene-derived UCH-L1 proteins in spermatogonia (Sg, arrowheads) and Sertoli cells (Se, arrows) but not in the primary spermatocytes (Sc, white arrowheads; Tg22). Magnification: ×400. Scale bar, 50 μm.

cells in the testes of non-Tg males; however, localization was not apparent around pachytene spermatocytes or round, elongated spermatids (Fig. 2A). This distribution of UCH-L1 is in good agreement with previous reports (Kon et al., 1999; Kwon et al., 2004a). Compared with non-Tg males, overexpression of UCH-L1 in seminiferous tubules of Tg males (Tg21 and Tg22) occurred predominantly in spermatogonia and Sertoli cells, and was weakly positive or negative in spermatocytes (Fig. 2C,D). These data coincided with strong induction of the *Uchl1* transgene. Tg mice expressed a higher level of total UCH-L1 (both endogenous and exogenous), suggesting a correlation between excess UCH-L1 and sterility.

Morphological Examination

Histopathological analysis of testes from 6-month-old Tg21 and Tg22 revealed terminal loss of differentiated germ cells and a large number of pachytene spermatocytes that had degenerated (with condensed nuclei and giant cells) and been sloughed off, forcing an altered structure of the seminiferous tubules such that they appeared almost empty (Fig. 3A). The deformed seminiferous tubules also contained numerous arrested spermatocytes (Fig. 3A, arrowheads) and multinucleated giant cells (arrows). In contrast, the seminiferous tubules of *gad* mice were nearly intact, as in non-Tg males (data not shown). In non-Tg males, seminiferous tubules containing elongated spermatids in the inner layer were readily detected (data not shown), whereas these tubules were scarcely detectable in Tg21 (Fig. 3A) and Tg22. On the other hand, the four female Tg mice displayed a variety of phenotypes, including an increased number of apoptotic oocytes and granulosa cells relative to non-Tg females, leading to infertility (data not shown).

In non-Tg (Fig. 3B) and *gad* mice (Fig. 3C), only a few TUNEL-positive cells were identified, located at the periphery of the tubule. However, many fewer TUNEL-positive cells were detected in the Tg males (Fig. 3D,E), and cell morphology indicated that most of these positive cells were primary spermatocytes. However, neither the TUNEL assay nor microscopy revealed evidence of apoptosis in spermatogonia or Sertoli cells. We quantitatively assessed germ cell apoptosis in Tg, non-Tg, and *gad* mice by calculating the number of apoptotic cells per tubules in each testis. This value was 25 times higher in Tg testes compared with non-Tg or *gad* testes (the averages $\pm$ SD were as follows: 553 ± 72, $n = 2$ in Tg testes; 22 ± 4.2, $n = 3$ in non-Tg; and 21 ± 5.3, $n = 3$ in *gad*). The percentage of apoptosis-positive tubules in Tg testes was also significantly higher than in non-Tg or *gad* mice (the averages $\pm$ SD were as follows: 95.3 ± 2.7, $n = 2$ in Tg testes; 7.4 ± 2.2, $n = 3$ in non-Tg; and 7.1 ± 1.8, $n = 3$ in *gad*).

A control section of caput epididymis, an androgen-dependent organ, from same Tg mice was investigated. No UCH-L1 overexpressing was detected, and no pathological symptoms could be observed in the epididymis (data not shown).

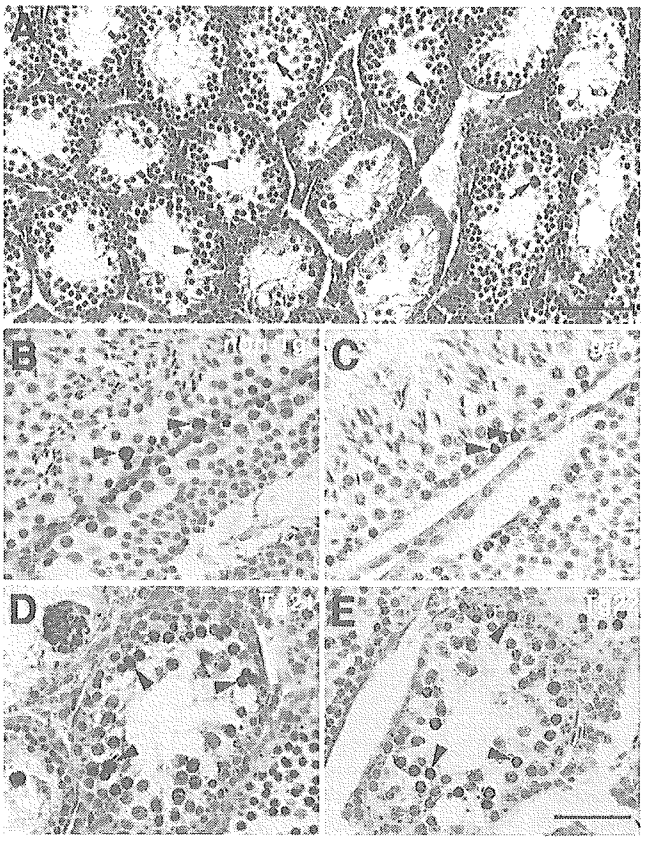

Fig. 3. Histopathology and TUNEL assay in situ. **A**: Hematoxylin–eosin staining of testis sections from the Tg21 male mouse shows defective spermatogenesis. Arrowheads indicate arrested spermatocytes and arrows indicate giant cells. Round spermatocytes and spermatids were rarely observed. **B–E**: Examples of TUNEL-positive cells characterized by the robust deposition of the reddish brown reaction product in sections of testis from non-Tg (B), *gad* (C), and Tg mice (D, Tg21; E, Tg22). Sections were counterstained with hematoxylin. A large number of TUNEL-positive cells were clearly observed at the periphery of the seminiferous tubule (arrowheads) in Tg21 (D) and Tg22 (E), whereas a lesser number of positives were apparent in non-Tg (B) or *gad* mice (C). Most of these positive cells appeared to be primary spermatocytes. Magnification: (A) ×100; (B–E) ×400. Scale bar in (A) 200 μm; (E) 50 μm.

UCH-L1 Relates to the Expression of PCNA

PCNA expression is associated with cell proliferation and DNA synthesis during S phase of the cell cycle and DNA repair in non-dividing cells (Kelman, 1997; Toschi and Bravo, 1988). Unlike UCH-L1, which is abundant in brain, PCNA is not detectable in the central nervous system (Saigoh et al., 1999; Williams et al., 2002). In the testis, PCNA is expressed in germ cells and Sertoli cells, and the nuclear localization of PCNA overlaps with that of UCH-L1 in monkey testis (Tokunaga et al., 1999). Our recent study showed that mice lacking UCH-L1 have significantly decreased numbers of PCNA-positive cells in seminiferous tubules (Kwon et al., 2003). These results led us to hypothesize that UCH-L1 may be closely associated with spermatogonial proliferation activity, possibly to maintain the primordial nature of these cells. We thus immunostained testes for PCNA

and UCH-L1. In non-Tg and *gad* testes, PCNA-positive staining was confined to spermatogonia and primary spermatocytes and was not evident in Sertoli cells (Fig. 4A,D,B,E) Similarly, the percentage of PCNA-positive spermatogonia and spermatocytes in the seminiferous tubules of *gad* mice was significantly lower than that of non-Tg mice (Fig. 4A,D,B,E) as we previously observed (Kwon et al., 2003). In contrast, Tg mouse testes showed greater PCNA staining in these cells; surprisingly however, staining was observed in nearly all arrested primary spermatocytes but not in spermatogonia (Fig. 4F). These findings suggest that UCH-L1 plays a specific role in mitotic proliferation. To further clarify the effect of UCH-L1 on PCNA levels, FLAG-tagged *Uchl1* was transfected into GC-1, a germ cell line derived from type B spermatogonia (Hofmann et al., 1992). UCH-L1 (anti-FLAG, Fig. 4G,I, green) and PCNA (Fig. 4H,I, red) were then visualized using immunofluorescence microscopy. Cells transfected with *Uchl1* showed lower PCNA immunoreactivity compared with mock-transfected cells (Fig. 4G), consistent with the assertion that PCNA is downregulated by UCH-L1 in vivo. However, no change of PCNA level was observed in *Uchl3* transfected cells (data not shown),

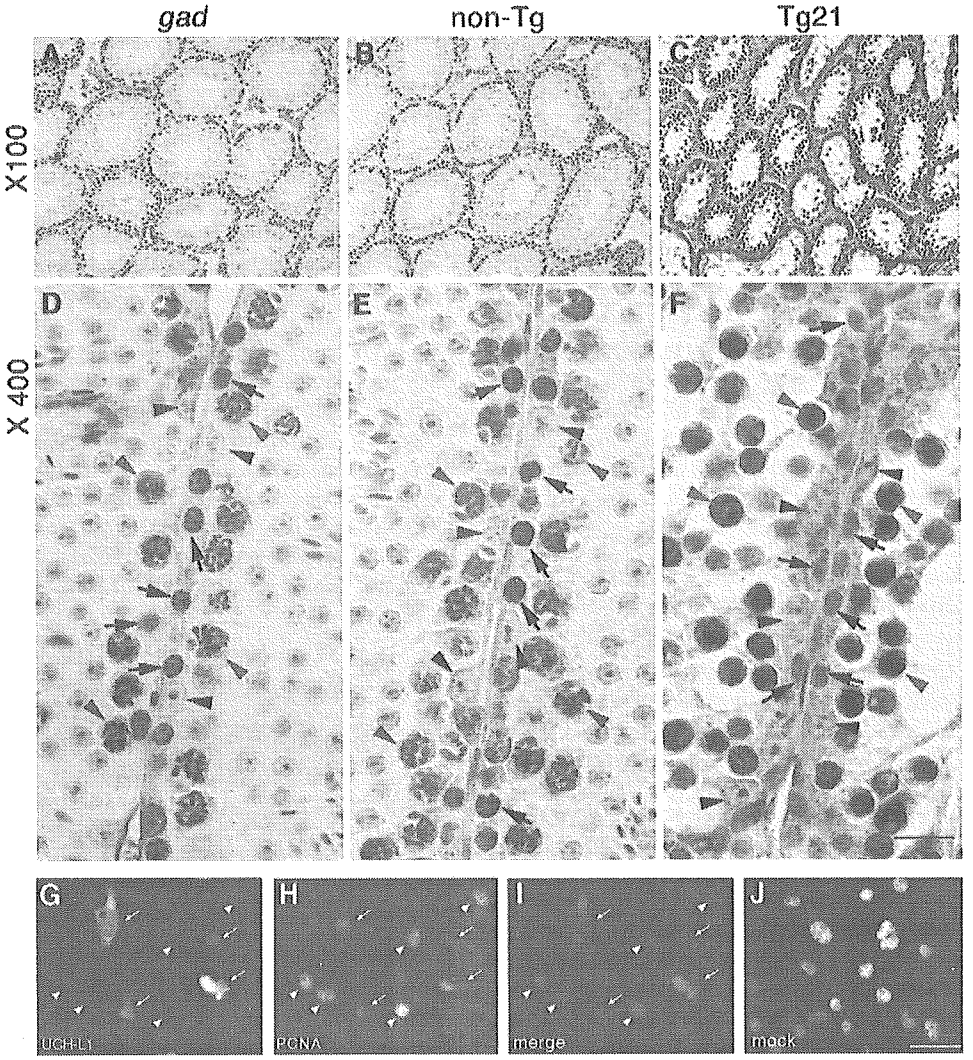

Fig. 4. PCNA immunostaining in the testes of a *gad* mouse (**A**, **D**), a non-Tg mouse (**B**, **E**), a Tg mouse (**C**, **F**; Tg21), and in the transient transfection assay with UCH-L1 using GC-1 cells (**G–J**). In *gad* and non-Tg testes, positive immunostaining was confined to spermatogonia (D, E; black arrows) and primary spermatocytes (D, E; red arrowheads), and staining was not seen in Sertoli cells (D, E; black arrowheads). In contrast, cell staining was more intense in the testis of Tg mice; however, this intensity was observed in almost all arrested primary spermatocytes (F; red arrowheads) but not in spermatogonia (F; black arrows). The staining of non-Tg and *gad* mice was essentially identical. However, nearly all the primary spermatocytes from Tg mice had relatively strong reactivity compared with spermatogonia that had very faint PCNA reactivity (black arrows). Plasmid pCIneo-*Uchl1* (G–I) or vector alone (J, mock) was transfected into GC-1 cells and expressed. Antibodies against FLAG (Sigma, monoclonal) and PCNA (BD Transduction Laboratory, polyclonal) were used to detect exogenously expressed UCH-L1 (G, I, green) and endogenous PCNA (H, J, I, red), respectively. Cells expressing a high level of UCH-L1 (G, white arrows) had a relative low level of PCNA (H, white arrows), whereas cells expressing a low level of UCH-L1 (H, white arrowheads) had high PCNA levels (H, white arrowheads). Magnification: (A–C) ×100; (D–J) ×400. Scale bar: **Upper panels** (see **panel C**), 200 μm; **middle panels** (see **panel F**), 50 μm; **lower panels** (see **panel J**), 50 μm.

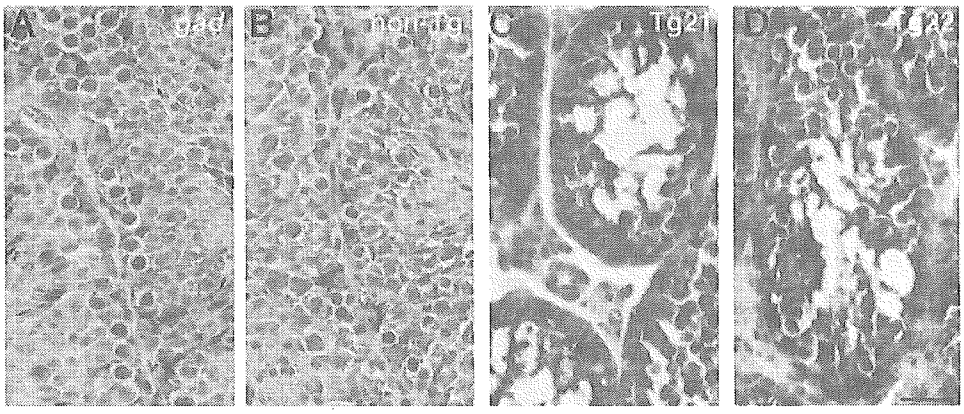

Fig. 5. Vimentin immunostaining in the testes of a *gad* mouse (**A**), a non-Tg mouse (**B**), and Tg mice (**C**, Tg21; **D**, Tg22). No difference was observed in the pattern and density of vimentin staining in Sertoli cells between *gad* (A) and non-Tg testes (B). In contrast, Sertoli cell staining was more intense in the Tg mice (C, D). Magnification: ×400. Scale bar, 200 μm.

suggesting the specificity of UCH-L1 effect on PCNA levels.

Sertoli Cells Exhibit High-Level Vimentin Expression in Tg Mice

We examined the immunoreactivity to vimentin, which is a marker of Sertoli cells (Oke and Suarez-Quian, 1993; Mori et al., 1997). Vimentin immunostaining was observed in Sertoli cells, and there is no difference between *gad* and non-Tg mice (Fig. 5A,B). In contrast, very strong expression of vimentin was observed in almost all Sertoli cells throughout the cytoplasm in Tg mice (Fig. 5C,D).

Bcl-2 Downregulation and Caspase-3 Upregulation in Tg Mice

The two key proteins, Bcl-2 and caspases-3 that involved in testicular germ cell apoptosis are especially altered during spermatogenesis or stress-induced germ cell apoptosis in *gad*mice (Harada et al., 2004; Kwon et al., 2004b, 2005). We thus examined the expression of these proteins in Tg and non-Tg testes to determine whether they are actually involved in countering increased apoptosis. Bcl-2 expression was downregulated in the testes of Tg mice compared with non-Tg mice (Fig. 6). In contrast to non-Tg mice, Tg mice had an elevated level of the activated caspase-3 subunit, p17 (Fig. 6), controversial to that observed in the retina of *gad* mice after ischemic injury (Harada et al., 2004). These results are consistent with the profound difference in UCH-L1 expression in these two mouse lines.

Upregulations of both Mono- and Poly-Ubiquitin in Tg Mice

Our recent studies suggested novel functions for UCH-L1, namely that it effectively upregulates ubiquitin levels at the post-transcriptional level (Osaka et al., 2003) and that ubiquitin induction plays a critical role in regulating cell death during cryptorchid injury–mediated germ cell apoptosis (Kwon et al., 2004b). Moreover, the testes of mice expressing K48R mutant ubiquitin are protected from cryptorchid injury (Rasoulpour et al., 2003). Given this information, we examined ubiquitin levels in *Uchl1* Tg mice. As expected, ubiquitin expression was strong in testicular cells of Tg mice (Fig. 7C,D), particularly in the arrested spermatocytes, but its expression was low in *gad* mice (Fig. 7B) compared with non-Tg mice (Fig. 7A). These data provide additional evidence that ubiquitin expression is induced upon UCH-L1 overexpression. To determine whether the increased ubiquitin staining represented monoubiquitin or polyubiquitin, we next examined the levels of both ubiquitin forms via immunoblotting (Fig. 7E). As expected, mono- and poly-ubiquitin levels in Tg mice were substantially higher than in non-Tg mice. A *gad* mouse control had relatively low levels

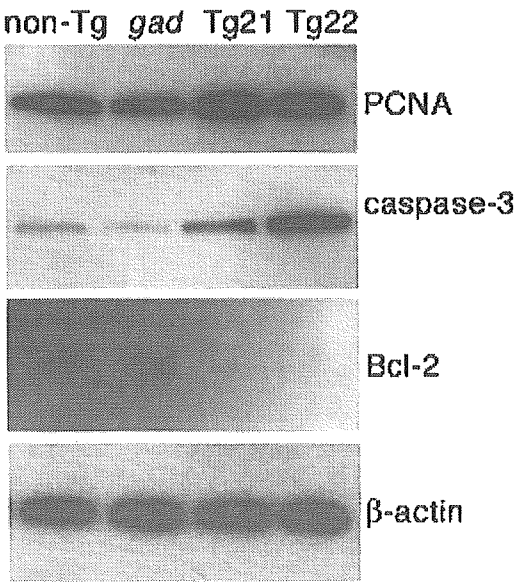

Fig. 6. Western blot analysis of Tg mouse testicular lysates. Consistent with the immunohistochemistry results, PCNA and caspase-3 substantially accumulated in Tg mice. However, the expression of antiapoptotic Bcl-2 decreased compared with non-Tg or *gad* mice.

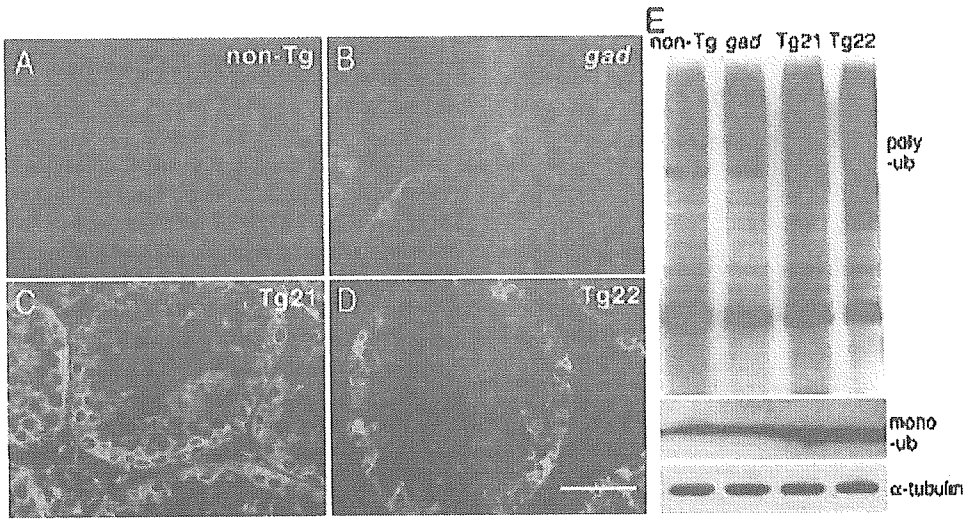

Fig. 7. The levels of mono- and poly-ubiquitin in the testes of non-Tg and Tg males. Double immunostaining for UCH-L1 and ubiquitin in the testis (**A**, non-Tg; **B**, *gad*; **C**, Tg21; **D**, Tg22). All strongly UCH-L1-positive cells (green) were also strongly positive for ubiquitin (red) in the two male Tg mice. Scale bar, 50 μm. **E**. An immunoblot showing that both mono- and poly-ubiquitin expression were significantly increased in the two Tg mice compared with non-Tg and *gad* mice (ub, ubiquitin).

of both mono- and poly-ubiquitin (Fig. 7E). These findings are consistent with previous studies and support the hypothesis that UCH-L1-mediated spermatocyte apoptosis involves the induction of ubiquitin expression.

DISCUSSION

Apoptosis in testicular germ cells is regulated by a complicated signal transduction pathway; however, the molecular mechanisms regulating this process are uncertain. We recently showed that *gad* mice, lacking UCH-L1 function, are resistant to apoptotic stress (Harada et al., 2004; Kwon et al., 2004b). These observations conclusively indicate that UCH-L1 plays a role in germ cell death during experimental stress-induced apoptosis. We thus hypothesized that germ cell apoptosis is directly induced by excess UCH-L1. To test this hypothesis, we utilized three mouse lines, wild-type (non-Tg), *gad* and *Uchl1* Tgs, which differ with respect to UCH-L1 expression. In Tg mice, germ cell apoptosis was barely detectable in spermatogonia or Sertoli cells, both of which strongly expressed UCH-L1. Apoptosis was observed mainly in primary spermatocytes, which had weak or negative UCH-L1 expression although they are derived from spermatogonia. These data suggest that excess UCH-L1 in fact does not directly induce apoptosis in spermatogonia or somatic Sertoli cells. These data further provoke the question of why apoptosis occurs during spermatocyte meiosis.

In our *Uchl1* Tg mice, there was no evidence of spermatogonia or Sertoli cell apoptosis despite the fact that these cells had stronger UCH-L1 expression compared with non-Tg mice. Accordingly, it could be concluded that overexpression of UCH-L1 in spermatogonia does not directly induce apoptosis in these cells (nor in Sertoli cells). Because spermatocytes are genetically distinct from the original mother cell (spermatogonia), we speculate that the Tg mice are highly susceptible to spermatocyte apoptosis in vivo, with the inference that spermatocytes seem to be particularly sensitive to UCH-L1 overexpression in spermatogonia even though spermatocytes themselves express a much lower level of UCH-L1. In contrast, *gad* mice are resistant to cryptorchid-induced germ cell apoptosis, and many germ cells undergo apoptosis in older animals although their testes develop nearly normally and produce mature sperm (Kwon et al., 2004b). These data suggest that the lack of UCH-L1 causes mice to have lower sensitivity to stress compared with wild-type males, although UCH-L1 is probably not essential for spermatogenesis under normal conditions. On one hand, UCH-L1 seems to be necessary for the stabilization of germ cells to protect against aging-associated apoptosis; however, the stabilization of germ cells appears to be limited by the concentration of UCH-L1, and consequently they may be damaged during spermatocyte meiosis when UCH-L1 is overexpressed. Despite the fact that excess UCH-L1 does not induce spermatogonial apoptosis, abnormalities in intracellular regulatory factors may potentially influence mitosis directly (i.e., as the cell divides into two daughter cells—spermatocytes). Some of these factors may accumulate or be reduced in the presence of excess UCH-L1, thereby causing disruptions such as arrested meiosis or the onset of apoptosis in spermatocytes rather than spermatogonia (Fig. 8).

Many of the factors involved in cellular apoptosis, including the Bcl-2 family and caspases, are targets for ubiquitynation. Previously, we have shown that Bcl-2 is upregulated (Kwon et al., 2004b) and caspases-3 is downregulated (Kwon et al., 2005) in *gad* mice. The decreased level of Bcl-2 and increased level of caspases-3

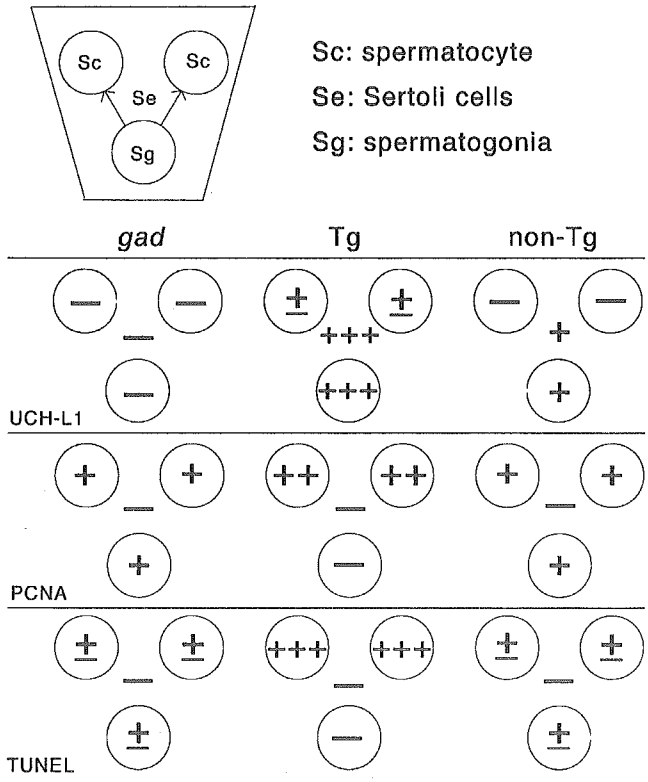

Fig. 8. TUNEL activity, and UCH-L1 and PCNA immunoreactivities in seminiferous tubules of non-Tg, *gad* and Tg mice. TUNEL activity or immunoreactivity: +++, strong; ++, moderate; + to ±, low to weak; –, not detectable.

observed in Tg mice in this study suggest that UCH-L1 can regulates the apoptosis during spermatogenesis by influencing the balance between apoptotic and anti-apoptotic proteins.

PCNA is ubiquitylated at lysine 48 (K48) and degraded by the ubiquitin-proteasome system (Yamamoto et al., 2004). In addition, PCNA is also monoubiquitylated at K164, thereby priming K63-linked polyubiquitin chains, which unlike K48-linked chains, do not promote proteasomal degradation (Hoege et al., 2002). In our present study, excess UCH-L1 relocalized PCNA from spermatogonia to spermatocytes and Sertoli cells in vivo and reduced PCNA expression to a low level in vitro. Based on these data, we hypothesize that UCH-L1, at least in part, may influence germ cell meiosis by affecting PCNA ubiquitynation, thereby disrupting its localization. In fact, PCNA significantly accumulated in primary spermatocytes of Tg mice (Fig. 4F). Since we did not obtain data regarding PCNA ubiquitylation in Tg mice, it is not clear whether the accumulated PCNA we observed was monoubiquitylated or polyubiquitylated. In any case, the accumulation of PCNA in primary spermatocytes may alter, damage or interrupt physical functions during meiosis (Fig. 8).

Germ cells and Sertoli cells are the only cell types expressed inside seminiferous tubules (McLaren, 1998). Germ cells constitute the male meiotic contribution to the reproductive cycle, whereas Sertoli cells support the growth and differentiation of germ cells. Direct interaction between germ cells and Sertoli cells may constitute an important part of the regulation of spermatogenesis (Russell et al., 1993). Indeed, mice exposed to Sertoli cell toxicants exhibit increased germ cell apoptosis (Lee et al., 1999). Therefore, Sertoli cells play a special role in nurturing and controlling spermatogenesis. Until postnatal day 16, UCH-L1 localizes only to spermatogonia, whereas after day 30 it also appears in Sertoli cells (Kon et al., 1999). Therefore, although UCH-L1 is highly expressed in both spermatogonia and somatic Sertoli cells, its function may be cell type-dependent. Under normal conditions UCH-L1 is a marker for activated Sertoli cells, in which it plays an important role in the degradation of abnormal proteins via the ubiquitin-proteasome system (Kon et al., 1999). Thus, we suspect that germ cell apoptosis in Tg mice might be related to the abnormal physical conditions in these cells. Our present work demonstrates that Tg mouse Sertoli cells are intensely immunoreactivity for UCH-L1, as expected. Furthermore, with vimentin, which is a marker present only in Sertoli cells (Oke and Suarez-Quian, 1993; Mori et al., 1997), we showed in this study that Tg mice had more vimentin immunoreactivity than non-Tg or *gad* mice (Fig. 5). Thus, forced expression of UCH-L1 in Sertoli cells perhaps may lead to gain of UCH function, thereby interrupting Sertoli cell-germ cell interactions that in turn promote germ cell apoptosis (Fig. 8).

In conclusion, we have demonstrated that UCH-L1 is an important spermatogenic factor related to PCNA and ubiquitin function. We used Tg mice overexpressing UCH-L1 to identify a new role for this protein. Overexpression of the *Uchl1* transgene inhibited spermatogenesis and induced germ cell death via an apoptotic mechanism, leading to male sterility. To our knowledge, the present data constitute the first description of a proapoptotic role for UCH-L1 in *Uchl1* Tg mice, as clearly revealed by the morphological and TUNEL results. Although UCH-L1 is constitutively expressed during spermatogenesis, and spermatogenic cell apoptosis is a normal aspect of mammalian spermatogenesis (Allan et al., 1992; Furuchi et al., 1996), the frequent cell death found in our *Uchl1* Tg mice could reflect an exaggeration of naturally occurring apoptosis. However, at present we do not understand whether the *Uchl1* transgene acts solely by inducing apoptosis or by interfering with differentiation so as to cause germ cell loss. This issue must be addressed to more fully define the role of UCH-L1 in the regulation and fate of spermatogonia during spermatogenesis.

ACKNOWLEDGMENTS

We thank H. Kikuchi for assistance in preparing the sections and M. Shikama for the care and breeding of animals.

REFERENCES

Allan DJ, Harmon BV, Roberts SA. 1992. Spermatogonial apoptosis has three morphologically recognizable phases and shows no circadian

rhythm during normal spermatogenesis in the rat. Cell Prolif 25: 241–250.
Aoki S, Su Q, Li H, Nishikawa K, Ayukawa K, Hara Y, Namikawa K, Kiryu-Seo S, Kiyama H, Wada K. 2002. Identification of an axotomy-induced glycosylated protein, AIGP1, possibly involved in cell death triggered by endoplasmic reticulum-Golgi stress. J Neurosci 22: 10751–10760.
Baarends WM, van der Laan R, Grootegoed JA. 2000. Specific aspects of the ubiquitin system in spermatogenesis. J Endocrinol Invest 23: 597–604.
Furuchi T, Masuko K, Nishimune Y, Obinata M, Matsui Y. 1996. Inhibition of testicular germ cell apoptosis and differentiation in mice misexpressing Bcl-2 in spermatogonia. Development 122: 1703–1709.
Harada T, Harada C, Wang YL, Osaka H, Amanai K, Tanaka K, Takizawa S, Setsuie R, Sakurai M, Sato Y, Noda M, Wada K. 2004. Role of ubiquitin carboxy terminal hydrolase-L1 in neural cell apoptosis induced by ischemic retinal injury in vivo. Am J Pathol 164:59–64.
Hoege C, Pfander B, Moldovan GL, Pyrowolakis G, Jentsch S. 2002. RAD6-dependent DNA repair is linked to modification of PCNA by ubiquitin and SUMO. Nature 419:135–141.
Hofmann MC, Narisawa S, Hess RA, Millan JL. 1992. Immortalization of germ cells and somatic testicular cells using the SV40 large T antigen. Exp Cell Res 201:417–435.
Imai T, Kawai Y, Tadokoro Y, Yamamoto M, Nishimune Y, Yomogida K. 2004. In vivo and in vitro constant expression of GATA-4 in mouse postnatal Sertoli cells. Mol Cell Endocrinol 214:107–115.
Kelman Z. 1997. PCNA: Structure, functions, and interactions. Oncogene 14:629–640.
Kon Y, Endoh D, Iwanaga T. 1999. Expression of protein gene product 9.5, a neuronal ubiquitin C-terminal hydrolase, and its developing change in sertoli cells of mouse testis. Mol Reprod Dev 54:333–341.
Kroll KL, Amaya E. 1996. Transgenic *Xenopus* embryos from sperm nuclear transplantations reveal FGF signaling requirements during gastrulation. Development 122:3173–3183.
Kurihara LJ, Kikuchi T, Wada K, Tilghman SM. 2001. Loss of Uch-L1 and Uch-L3 leads to neurodegeneration, posterior paralysis, and dysphagia. Hum Mol Genet 10:1963–1970.
Kwon J, Kikuchi T, Setsuie R, Ishii Y, Kyuwa S, Yoshikawa Y. 2003. Characterization of the testis in congenitally ubiquitin carboxy-terminal hydrolase-1 (Uch-L1) defective (gad) mice. Exp Anim 52: 1–9.
Kwon J, Wang YL, Setsuie R, Sekiguchi S, Sakurai M, Sato Y, Lee WW, Ishii Y, Kyuwa S, Noda M, Wada K, Yoshikawa Y. 2004a. Developmental regulation of ubiquitin C-terminal hydrolase isozyme expression during spermatogenesis in mice. Biol Reprod 71: 515–521.
Kwon J, Wang YL, Setsuie R, Sekiguchi S, Sato Y, Sakurai M, Noda M, Aoki S, Yoshikawa Y, Wada K. 2004b. Two closely related ubiquitin C-terminal hydrolase isozymes function as reciprocal modulators of germ cell apoptosis in cryptorchid testis. Am J Pathol 165:1367–1374.
Kwon J, Mochida K, Wang YL, Sekiguchi S, Sankai T, Aoki S, Ogura A, Yoshikawa Y, Wada K. 2005. Ubiquitin C-terminal hydrolase L-1 is essential for the early apoptotic wave of germinal cells and for sperm quality control during spermatogenesis. Biol Reprod 73:29–35.
Lee J, Richburg JH, Shipp EB, Meistrich ML, Boekelheide K. 1999. The Fas system: A regulator of testicular germ cell apoptosis, is differentially up-regulated in Sertoli cell versus germ cell injury of the testis. Endocrinology 140:852–858.
Matzuk MM, Lamb DJ. 2002. Genetic dissection of mammalian fertility pathways. Nat Cell Biol 4:s41–s49.
McLaren A. 1998. Gonad development: Assembling the mammalian testis. Curr Biol 8:R175–R177.
Mizushima S, Nagata S. 1990. pEF-BOS: A powerful mammalian expression vector. Nucleic Acids Res 18:5322.
Mori C, Nakamura N, Dix DJ, Fujioka M, Nakagawa S, Shiota K, Eddy EM. 1997. Morphological analysis of germ cell apoptosis during postnatal testis development in normal and Hsp 70-2 knockout mice. Dev Dyn 208:125–136.
Oke BO, Suarez-Quian CA. 1993. Localization of secretory, membrane-associated, and cytoskeletal proteins in rat testis using an improved immunocytochemical protocol that employs polyester wax. Biol Reprod 48:621–631.
Osaka H, Wang YL, Takada K, Takizawa S, Setsuie R, Li H, Sato Y, Nishikawa K, Sun YJ, Sakurai M, Harada T, Hara Y, Kimura I, Chiba S, Namikawa K, Kiyama H, Noda M, Aoki S, Wada K. 2003. Ubiquitin carboxy-terminal hydrolase L1 binds to and stabilizes monoubiquitin in neuron. Hum Mol Genet 12:1945–1958.
Osawa Y, Wang YL, Osaka H, Aoki S, Wada K. 2001. Cloning, expression, and mapping of a mouse gene, *Uchl4*, highly homologous to human and mouse Uchl3. Biochem Biophys Res Commun 283: 627–633.
Rasoulpour RJ, Schoenfeld HA, Gray DA, Boekelheide K. 2003. Expression of a K48R mutant ubiquitin protects mouse testis from cryptorchid injury and aging. Am J Pathol 163:2595–2603.
Russell LD, Corbin TJ, Borg KE, De Franca LR, Grasso P, Bartke A. 1993. Recombinant human follicle-stimulating hormone is capable of exerting a biological effect in the adult hypophysectomized rat by reducing the numbers of degenerating germ cells. Endocrinology 133:2062–2070.
Saigoh K, Wang YL, Suh JG, Yamanishi T, Sakai Y, Kiyosawa H, Harada T, Ichihara N, Wakana S, Kikuchi T, Wada K. 1999. Intragenic deletion in the gene encoding ubiquitin carboxy-terminal hydrolase in gad mice. Nat Genet 23:47–51.
Sutovsky P. 2003. Ubiquitin-dependent proteolysis in mammalian spermatogenesis, fertilization, and sperm quality control: Killing three birds with one stone. Microsc Res Tech 61:88–102.
Tokunaga Y, Imai S, Torii R, Maeda T. 1999. Cytoplasmic liberation of protein gene product 9.5 during the seasonal regulation of spermatogenesis in the monkey (*Macaca fuscata*). Endocrinology 140:1875–1883.
Toschi L, Bravo R. 1988. Changes in cyclin/proliferating cell nuclear antigen distribution during DNA repair synthesis. J Cell Biol 107: 1623–1628.
Wilkinson KD. 2000. Ubiquitination and deubiquitination: Targeting of proteins for degradation by the proteasome. Semin Cell Dev Biol 11:141–148.
Williams K, Schwartz A, Corey S, Orandle M, Kennedy W, Thompson B, Alvarez X, Brown C, Gartner S, Lackner A. 2002. Proliferating cellular nuclear antigen expression as a marker of perivascular macrophages in simian immunodeficiency virus encephalitis. Am J Pathol 161:575–585.
Wing SS. 2003. Deubiquitinating enzymes—the importance of driving in reverse along the ubiquitin-proteasome pathway. Int J Biochem Cell Biol 35:590–605.
Yamamoto T, Kimura S, Mori Y, Oka M, Ishibashi T, Yanagawa Y, Nara T, Nakagawa H, Hashimoto J, Sakaguchi K. 2004. Degradation of proliferating cell nuclear antigen by 26S proteasome in rice (*Oryza sativa* L.). Planta 218:640–646.
Yamazaki K, Wakasugi N, Tomita T, Kikuchi T, Mukoyama M, Ando K. 1988. Gracile axonal dystrophy (GAD): A new neurological mutant in the mouse. Proc Soc Exp Biol Med 187:209–215.
Yuan L, Liu JG, Zhao J, Brundell E, Daneholt B, Hoog C. 2000. The murine *SCP3* gene is required for synaptonemal complex assembly, chromosome synapsis, and male fertility. Mol Cell 5:73–83.

Available online at www.sciencedirect.com
SCIENCE DIRECT
ELSEVIER
Biochemical and Biophysical Research Communications 339 (2006) 717–725
BBRC
www.elsevier.com/locate/ybbrc

Characterization of multimetric variants of ubiquitin carboxyl-terminal hydrolase L1 in water by small-angle neutron scattering

Sachio Naito [a,b,*], Hideki Mochizuki [b], Toru Yasuda [b], Yoshikuni Mizuno [b], Michihiro Furusaka [c], Susumu Ikeda [c], Tomohiro Adachi [d], Hirohiko M. Shimizu [d], Junichi Suzuki [e], Satoru Fujiwara [e], Tomoko Okada [f], Kaori Nishikawa [f], Shunsuke Aoki [f], Keiji Wada [f]

[a] *High Energy Accelerator Research Organization, 1-1 Oho, Tsukuba-shi, Ibaraki 305-0801, Japan*
[b] *Department of Neurology, Juntendo University School of Medicine, 2-1-1 Hongo 113-8421, Tokyo, Japan*
[c] *Department of Mechanical Intelligence Engineering, Graduate School of Engineering, Hokkaido University, Kita 13, Nishi 8, Kita-ku, Sapporo 060-8628, Japan*
[d] *RIKEN, 2-1 Hirosawa, Wako, Saitama 351-0198, Japan*
[e] *Japan Atomic Energy Research Institute, 2-4 Tokaimura-shirakata-shirane, Naka-gun, Ibaraki 319-1195, Japan*
[f] *Department of Degenerative Neurological Diseases, National Institute of Neuroscience, National Centre of Neurology and Psychiatry, 4-1-1 Ogawa Higashi, Kodaira, Tokyo 187-8502, Japan*

Received 4 November 2005
Available online 21 November 2005

Abstract

Here, we illustrated that the morphological structures of ubiquitin carboxyl-terminal hydrolase L1 (UCH-L1) variants and Parkinson's disease (PD) exhibit good pathological correlation by a small-angle neutron scattering (SANS). UCH-L1 is a neuro-specific multiple functional enzyme, deubiquitinating, ubiquityl ligase, and also involved in stabilization of mono-ubiquitin. To examine the relationship between multiple functions of UCH-L1 and the configuration of its variants [wild-type, I93M (linked to familial Parkinson's disease), and S18Y (linked to reduced risk of Parkinson's disease)], in this report, we proposed that these were all self-assembled dimers by an application of a rotating ellipsoidal model; the configurations of these dimers were quite different. The wild-type was a rotating ellipsoidal. The globular form of the monomeric component deformed by the I93M mutation. Conversely, the S18Y polymorphism promoted the globularity. Thus, the multiple functional balance is closely linked to the intermolecular interactions between the UCH-L1 monomer and the final dimeric configuration.

Keywords: Small-angle neutron scattering; Ubiquitin carboxyl-terminal hydrolase L1; Structure in water; Parkinsonism

Although there are papers using neutron scattering to study the behavior of proteins in whole cells, this paper is actually about the conformation of a protein in solution. The crystal structure analysis of proteins by X-ray has advanced our understanding of the correlation between biological function and structure. Small-angle X-ray scattering and neutron scattering are useful analytical methods to determine the configuration of proteins in water, such as hen egg-white lysozyme [1,2], myoglobin, hemoglobin, α-lactalbumin, ribonuclease [3], and bovine serum albumin [4]. Recently, in the field of small- and wide-angle X-ray scattering measurement, intense X-ray beams became available at third-generation X-ray sources; however, radiation damage to biomacromolecules is acknowledged as a serious problem in modern structural biology at room temperature [5,6]. The reaction of the incident X-ray with water molecules creates hydroxyl or hydroperoxyl radicals that rapidly attach to the backbones

* Corresponding author. Fax: +81 29 856 3202.
E-mail address: sachio@post.kek.jp (S. Naito).

0006-291X/$ - see front matter © 2005 Elsevier Inc. All rights reserved.
doi:10.1016/j.bbrc.2005.11.066

and/or side chains of proteins. In many cases, the interactions between the radical-activated proteins give rise to radiation-induced aggregates connected to each other by covalent and/or non-covalent bonds, such as cystine bond [6–9].

On the other hand, neutron beam generated from a cold-neutron source causes less damage to protein solution. Small-angle neutron scattering (SANS) experiments can provide useful information regarding the aggregation number, shape, and dimensions of the structure [10]. The SANS technique has been applied to analyze the conformational changes in brain protein; amyloid β-protein fibrillation [11–13] because SANS allows observation of amyloid aggregates in Alzheimer's disease without the anxiety of artificial aggregation caused by X-ray radiation.

A topical and biologically important issue is the mechanism of protein metabolism in living cells through the proteasome system, ubiquitination, and deubiquitination. In particular, deubiquitination is considered essential for negative regulation of proteolysis and for recycling of ubiquitin from polyubiquitin chains [14]. Ubiquitin C-terminal hydrolase L1 (UCH-L1) is an abundant multi-functional neuronal enzyme (1–2% of brain-soluble proteins [15]) involved in deubiquitination [14], ubiquityl ligase activity varied by the oligomerization in an aqueous solution [16], and stabilization of mono-ubiquitin [17,18]. The disordered neuronal functions linked to Parkinson's disease (PD) may be associated with accumulation of unnecessary proteins in cells by a dysfunctional proteasome system. The partial loss of UCH-L1 hydrolase activity in an I93M missense mutant may contribute to the disease [15]. Furthermore, an S18Y polymorphism may be associated with decreased risk of PD in Caucasian, German, and Japanese populations [19–23]. The aim of this study was to clarify whether UCH-L1 variants exist as a monomer or multimer in water without adding any chemical and physical modifications to the cysteine hydrolase and, in particular, to discuss the relation between the configuration of the variants and the risk of PD.

Materials and methods

UCH-L1 variants preparation. Wild-type, I93M, S18Y, and I93/S18Y double-substituted recombinant proteins were cloned, expressed in *Escherichia coli*, and purified, as previously described [24]. Protein concentrations were determined using the BCA protein assay reagent (Pierce). The purified proteins were resolved by SDS–PAGE (sodium dodecyl sulfate–polyacrylamide gel electrophoresis) under reducing conditions and visualized by Coomassie brilliant blue R-250 to confirm the purity. Each variant (0.85 mg) was dissolved into 1 ml of 40 mM Hepes buffer in deuterized water (D_2O) containing 5 mM dithiothreitol and 0.5 mM EDTA.

Small-angle neutron scattering. Small-angle neutron scattering was undertaken at the High Energy Accelerator Research Organization using a wide-angle neutron diffractometer (WINK) installed at the pulsed neutron scattering facility, Tsukuba, Japan. The energy of a cold neutron beam at λ is 0.5–16.1 Å, while the neutron wavelength using a SANS measurement by WINK installed at KEK, is ca. 11–80 meV. We obtained good scattering curves in the momentum-transfer q range of 0.03–0.15 $Å^{-1}$. Here, q is related to the Bragg angle (θ) by $q = (4\pi/\lambda)\sin\theta$. For every pair of solution and solvent, the scattering intensity was measured as a function of q and the transmissions for the neutron beam, T_{sol} and T_{solv}. After background (noise) and normalization corrections, intensity data recorded on the two-dimensional PSD were radially averaged, resulting in scattering functions of $I(q)_{soln}$ and $I(q)_{solv}$. The scattering for the solvent was subtracted from that of the solution based on Eq. (1).

$$I(q) = I(q)_{soln} - I(q)_{solv}(T_{soln}/T_{solv}). \quad (1)$$

SANS data analysis. We obtained homology modeling structure information [(the atomic coordinates of the protein in the Protein Data Bank (PDB)) of human UCH-L1 from the highly homologous (57.7% identity) human UCH-L3 crystal structure [25] using SWISS-MODEL [26–28]]. The theoretical radius of gyration ($Rg = 16.5$ Å) of UCH-L1 was calculated using the CRYSON program by Svergun [29,30] and the real radius, R, was calculated to be 21.5 Å ($R = \sqrt{5/3}Rg$). In this measurement, the concentration of UHC-L1 variants (0.85 mg/ml, corresponding to 34 μM) was sufficiently below C^*, the critical concentration, meaning that the molecules can disperse as a single molecule in a solvent. When a sphere protein having radius R disperses in a solution, the scattering intensity is described by

$$I(q) = \left(3\frac{\sin(qR) - qR\cos(qR)}{(qR)^3}\right)^2 \quad (2)$$

where q is the momentum transfer. However, the actual SANS curves of UCH-L1 variants reflected that of dimer rather than monomer. Then, we assumed the dispersion of monomeric or dimeric and rotating ellipsoidal particle (short axis, a; and long axis, b and c, $a \leqslant b = c$ or short axis, a and b; and long axis, c, $a = b \leqslant c$) and obtained theoretical SANS curves by applying the following equation of Debye [31] based on the scattering intensity from correlations between one or two non-spherical bodies:

$$I(q) = \sum_i \sum_j f_i f_j \frac{\sin(qr_{ij})}{qr_{ij}}, \quad (3)$$

where r_{ij} is the distance between any two points in the protein molecule, and f_i and f_j are the scattering lengths at each point. We assumed that the volume of the particle is retained even though the proportion of the long axis and the short one is changed. In the q range of the SANS measurement, we assumed a constant scattering factor in the UCH-L1 variants, and thus divided the rotating ellipse by the resolution of a 5 Å cube. We confirmed that the scattering curve of a spherical monomer obtained from Eq. (3) resembled that from Eq. (2). Therefore, Eq. (3) can be applied not only to the monomer but also the dimer. The scattering intensity, calculated from Debye's equation [31], was evaluated by the following equation:

$$R = \frac{\sum_q \{(mI_c(q) - n - I_c(q))q^2\}^2}{\sum_q (I_c(q)q^2)^2}, \quad (4)$$

where m is a scaling factor, n is a background factor, and $I_c(q)$ and $I_c(q)$ are the experimental and calculated scattering intensities, respectively. The factor, R, becomes minimum when the parameters, m and n, are changed [29,30].

Circular dichroism. Circular dichroism (CD) measurements were performed as described previously [24]. Purified recombinant human UCH-L1 and mutants were adjusted to a concentration of 8.7×10^{-4} M and dialyzed against a 20 mM Hepes buffer (pH 7.8). Far-UV CD spectra (195–250 nm) were recorded in a 1-mm quartz cuvette on a Jasco J-820 spectropolarimeter (Jasco, Tokyo, Japan) equipped with a temperature controller by scanning at a rate of 50 nm/min at 20 °C. For all spectra, six scans were averaged. All CD spectra were corrected by background subtraction of the spectrum obtained with the buffer alone and smoothed. The observed ellipticity was normalized to units of degrees cm^2 = dmol. The spectra were analyzed for percent secondary structural elements by a computer program based on an algorithm that compares the experimental spectra with those of known proteins [32].

Result

Characterization of purified recombinant human UCH-L1 proteins

To avoid artificial polymerisation among proteins by disulfide bonds, we carefully purified wild-type UCH-L1, I93M (linked to familial PD), and S18Y (linked to reduced risk of PD), and I93/S18Y double-substituted recombinant proteins (Fig. 1A) under reducing conditions as described previously [24]. SDS–PAGE showed a single 28.9-kDa band for each of the 6HN-tagged proteins (Fig. 1B) in good agreement with the theoretical 27.8-kDa molecular mass of the 6HN-tagged UCH-L1. The expression levels for the wild-type and variant UCH-L1 proteins were equivalent. The residue 93 is proximal to the active site (C90), while the location of residue 18 is on the protein surface, distal from the active site (Fig. 1C).

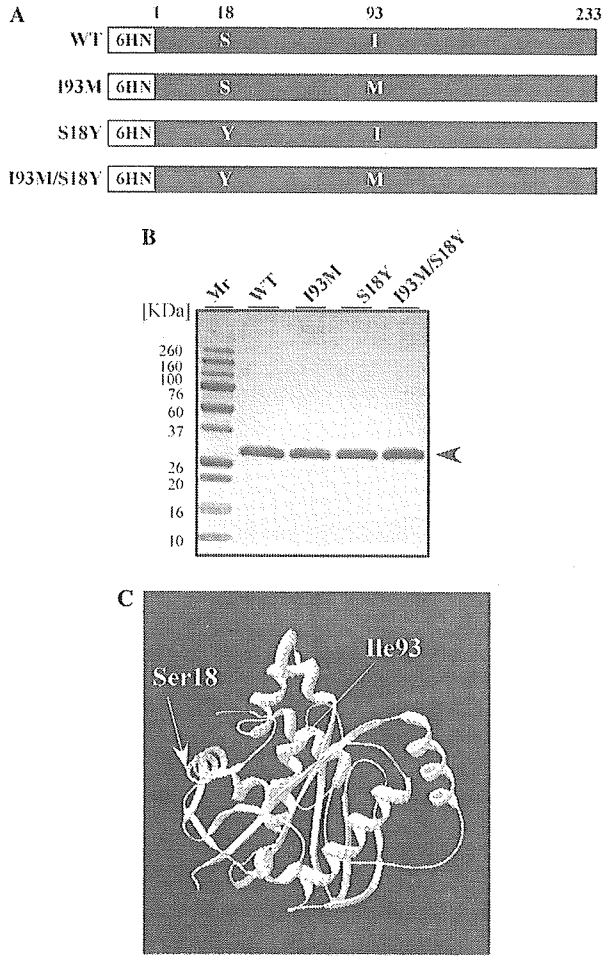

Fig. 1. Characterization and analysis of purified recombinant 6HN-tagged human UCH-L1s. (A) Schematic representation of 6HN-tagged human UCH-L1 wild-type (WT) and mutants I93M, S18Y, and I93/S18Y double-substituted recombinant. The numbers indicate the amino acid residues of the N- and C-termini of UCH-L1 (open reading frame). The positions of the point mutations are indicated. The N-terminal 6HN-tag is shown in white. (B) Visualization of recombinant human UCH-L1s by SDS–PAGE under reducing conditions and Coomassie staining. One microgram of each sample was subjected to analysis. The *arrow* indicates the 28.9-kDa 6HN-tagged human UCH-L1 bands. Mr, molecular weight markers (kDa). (C) The crystal structure of UCH L-1 was modeled after the crystal structure of human UCH-L3 [25] using SWISS-MODEL protein modeling [26–28]. The residue 93 is proximal to the active center (C90), while the location of residue 18 on the protein surface, distal from the active site.

SANS analysis of tertiary structure of wild-type and human UCH-L1 variants in water

SANS curves of a protein mostly reflect the characteristics of the aggregation number, shape, and dimensions of the structure. The experimental profile for the wild-type fitted well to the theoretical SANS curve (calculated from Eq. (2), based on the distance between the center of the two particles being 43 Å) of the dimer consisting of the two spherical monomers rather than that of the monomeric one ($R = 21.5$ Å) calculated from Eq. (2) (Fig. 2). We noted a rotating ellipsoidal monomer and dimer when the axis (a) was changed by the resolution of a 5 Å (Fig. 3A) and calculated the theoretical curves by Eq. (3) (Fig. 3B–D). The ambiguous difference between the theoretical SANS curves of the rotating ellipsoidal monomer (Fig. 3B) and the rotating ellipsoidal dimer (Fig. 3C) was observed in the q range of 0.03–0.1. However, $I(q)_{\text{dimer}}$ markedly diminished in the q range of 0.1–0.15, and then reached the first minimum value at $q = 0.15$, although the scattering intensity ($I(q)_{\text{monomer}}$), gradually declined with increasing q value. Thus, the characteristic decrease of the scattering intensity

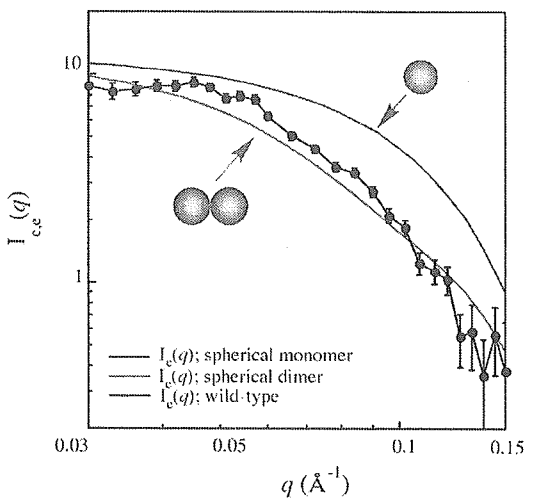

Fig. 2. The relative neutron scattering intensity ($I(q)$) versus the magnitude of the scattering vector q. $I_c(q)$ for the wild-type UCH-L1(black closed circle). The blue line indicates theoretical curves; $I_c(q)$, monomeric sphere (diameter = 21.5 Å calculated from Eq. (3), based on the R ($R = \sqrt{5/3}Rg$) value obtained using CRYSON program by Svergun [29,30]). The red line indicates theoretical curves; $I_c(q)$, dimeric spheres (calculated from Eq. (2), based on the distance between the center of the two particles being 43 Å).

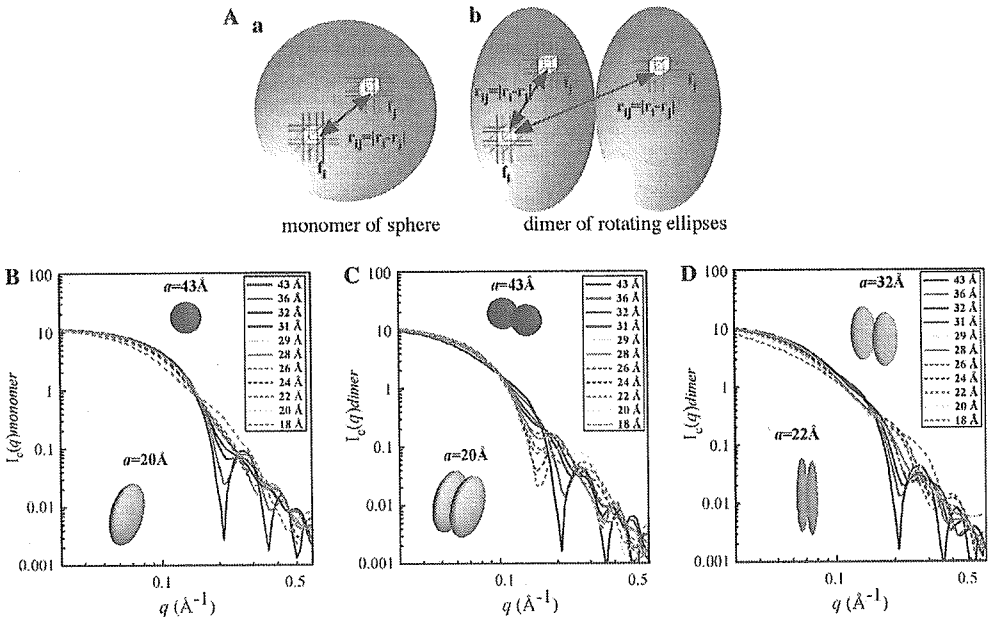

Fig. 3. Model calculations showing how ellipsoidal parameters affect the relative scattered intensity. (A) Schematic views of two body correlations. (a): monomer of a sphere. (b): dimer of rotating ellipses. In the q range of the SANS measurement, we assumed a constant scattering factor in the UCH-L1 variants, and thus divided the rotating ellipse by the resolution of a 5 Å cube. (B) $I_c(q)$ for the theoretical rotating ellipsoidal monomer, the remarks in the figure represent axis values of ellipsoid, e.g., when a is 20 Å, b and c are 62 Å. (C) $I_c(q)$ for the theoretical rotating ellipsoidal dimer (short axis, a; and long axis, b and c, $a \leqslant b = c$). (D) $I_c(q)$ for the theoretical rotating stick-like ellipsoidal dimer (short axis, a and b; and long axis, c, $a = b \leqslant c$), the remarks in the figure represent axis values of ellipsoid, e.g., When a and b are 22 Å, c is 164 Å. When a and b are 32 Å, c is 78 Å.

in the q range of 0.1–0.15 is observed on the SANS profiles of the rotating ellipsoidal dimers (short axis, a; and long axis, b and c, $a \leqslant b = c$), however, not observed on the rotating stick-like ellipsoidal dimer (short axis, a and b; and long axis, c, $a = b \leqslant c$) (Fig. 3D). The SANS profiles may provide the size of the rotating ellipsoidal dimers and therefore we applied this model to analyze the experimental SANS curves of UCH-L1 variants. The red lines in Fig. 4 are the best theoretical fits to a rotating ellipsoidal dimeric model determined individually for wild-type and each variant of UCH-L1s; the blue lines are those for a monomer having the same axis length. As shown in these figures, our data are consistent with this assumption in the q region. The wild-type is an ellipsoidal dimer [short axis, 29 Å; long axis, 52 Å (Fig. 4A)], the I93M mutant is also an ellipsoidal dimer [short axis, 20 Å; long axis, 62 Å (Fig. 4B)], the S18Y polymorphism is a spherical dimer [short axis, 43 Å; long axis, 43 Å (Fig. 4C)], and the I93M/S18Y double-substituted variant is an ellipsoidal dimer [short axis, 31 Å; long axis, 50 Å (Fig. 4D)]. The configuration of the aggregate was dependent on the monomeric protein structure caused by amino acid substitution. It is also quite clear that even the most deformed rotating ellipsoidal monomer never satisfies the experimental curve. The major component of UCH-L1 wild-type may exist as a dimer in water. These results imply that the most part of the wild-type and each UCH-L1 variant self-assembles and exists as a dimer in water. Thus, the fitting evaluation of the difference in the size and the shape between monomer and dimer is available by analyzing the SANS curve in the optimum q range.

To address whether the observed configurational differences of the UCH-L1 variants in water reflect on altered secondary structure, we used CD spectroscopy to estimate the secondary structure in the recombinant proteins (Fig. 5A). The ratios of α-helix, β-sheet, and other secondary structural features in these proteins were estimated from mean residue ellipticity data and are presented graphically in Fig. 5B. We previously indicated that relative to the wild-type, the I93M mutant displayed a slightly lower ellipticity over the range 195-200 nm, indicating a decreased α-helical content [24]. Relative to wild-type, the I93M substitution was also associated with the considerable increase in the content of β-sheet. On the other hand, the influence of the S18Y substitution on the variation of the secondary structures of UCHL-1 was smaller than that of I93M mutation, relative to the wild-type or the I93 mutant. However, the inclination was not only on the wild-type but also on the I93M mutant although the effect on increase of the β-turn content by the S18Y substitution of the amino acid sequence was small. These variations of the β-turn content were quite similar to those of the three-dimensional configuration of the ellipsoidal UCH-L1 based on SANS studies.

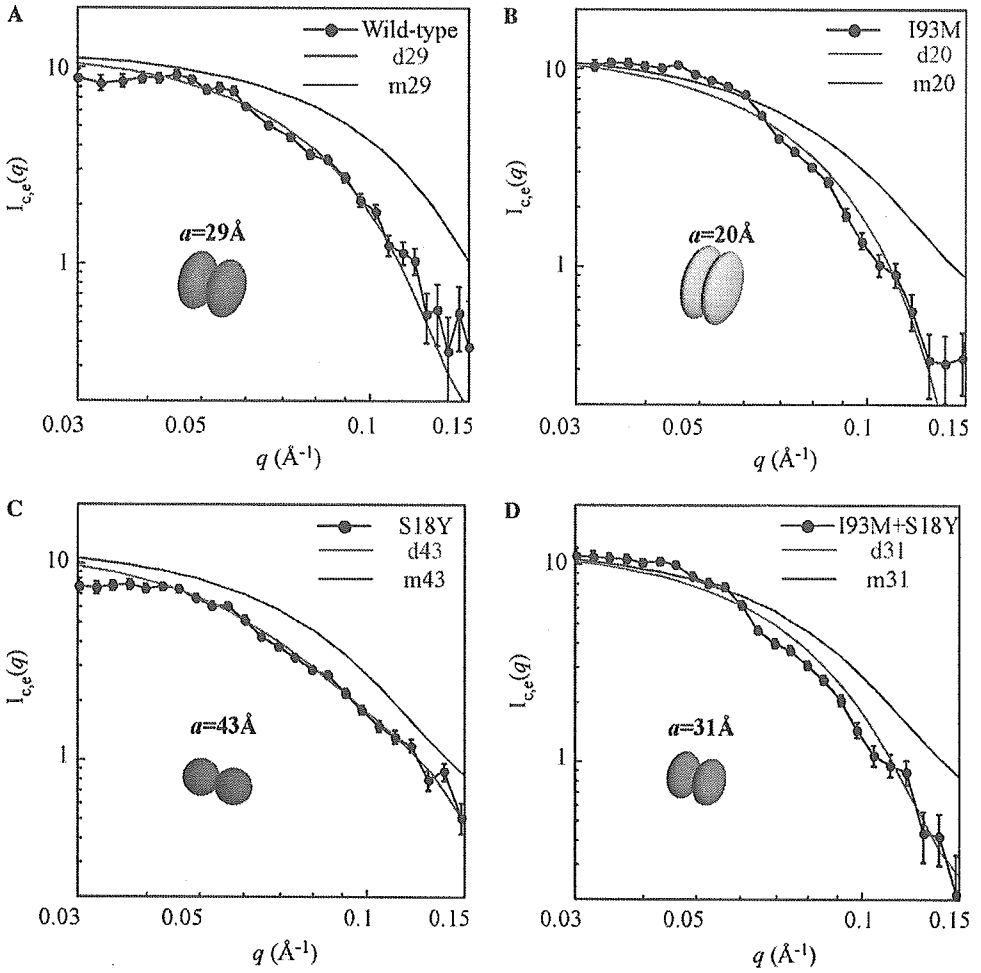

Fig. 4. Relative neutron scattering intensity $I(q)$ versus the magnitude of the scattering vector q. (A) $I_e(q)$ for the experimental curve of wild-type UCH-L1(black close circle). $I_c(q)$ for the calculated theoretical curves for dimer (d29) and monomer (m29). The red line corresponds to the theoretical fit for a rotating ellipsoidal dimer, (a, 29 Å; b, (=c), 52 Å). The blue line represents for a rotating ellipsoidal monomer having the same diameter. (B) $I_e(q)$ for the I93M mutant (black close circle). The red line corresponds to the theoretical fit for a rotating ellipsoidal dimer, (a, 20 Å, b, (=c), 62 Å). The blue line represents for the monomer. (C) $I_e(q)$ for the S18Y polymorphism (black close circle). The red line corresponds to the theoretical fit for a rotating spherical dimer, (a, 43 Å, b, (=c), 43 Å). The blue line represents for the monomer. (D) $I_e(q)$ for the I93M/S18Y double mutant (black close circle). The red line corresponds to the theoretical fit for rotating ellipsoidal dimer, (a, 31 Å, b, (=c), 50 Å). The blue line represents for the monomer.

Discussion

UCH-L1 is abundantly present neuronal brain protein enzyme with multiple enzymatic functions including hydrolysis of C-terminal ubiquityl esters, ubiquityl ligase activity, depending on multiple forms in an aqueous solution and stabilization of mono-ubiquitin. The aim of this study was to clarify whether UCH-L1 variants exist as a monomer or multimer in water and, in particular, to discuss the relation between the configuration of the variants and the risk of Parkinson's disease. We preferred SANS to address this question without adding any chemical modifications or physical force to proteins in water. We confirmed that no changes occurred on the SANS profiles of wild-type UCH-L1 and UCH-L1 variants during the measurement.

We first succeeded in demonstrating the configuration of UCH-L1 in an aqueous solution by SANS. The wild-type was a dimer, and the monomeric component was ellipsoidal, contrary to the expectation based on the crystal structure (Fig. 1C). The I93M variant was a dimer, and the monomeric component was more ellipsoidal than that of the wild-type. The protective polymorphic variant, S18Y, was also a dimer, but the configuration was quite different compared to wild-type and I93M, the monomeric component retained its spherical shape. The size-distribution of the UCH-L1 wild-type and variants is dependent on the concentration based on the time derivative analysis of the sedimentation velocity [16]. The 80% of the total wild-type is a monomer (~2.3S), ~15% is a dimer (4S), and ~5% is a tetramer (8S) at 7 μM. The populations of both oligomers increased with increased protein concentration, and the dimer became the predominant species at 70 μM. A similar concentration-dependent size growth was observed on S18Y; all of S18Y existed as a monomer at 10 μM, and

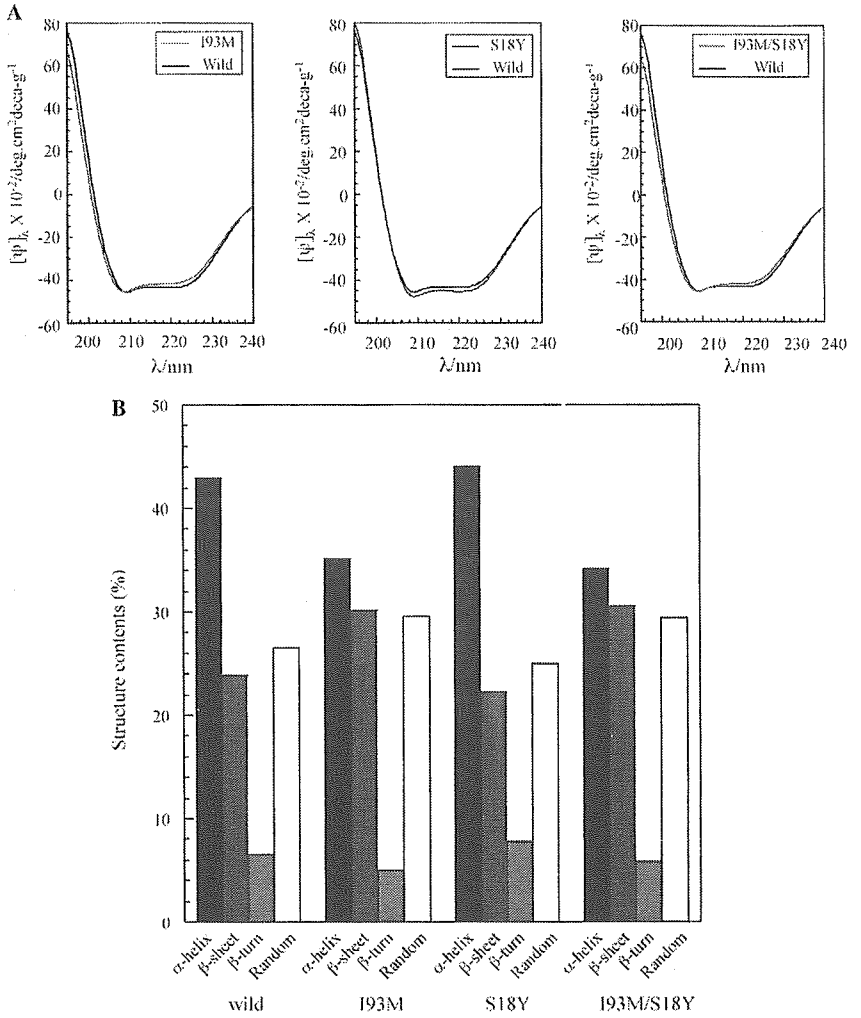

Fig. 5. CD spectra and secondary structural content of 6HN-tagged human UCH-L1s. CD spectra (mean residue ellipticity) for recombinant proteins (8.7×10^{-4} M) in a 20 mM Hepes buffer (pH 7.8). (A) Wild-type UCH-L1 is shown in black, I93M in red, S18Y in blue, and S18Y/I93M in green. (B) Secondary structural content of recombinant human 6HN-tagged UCH-L1s.

the dimer was detected at 28 μM. If homogeneity of the protein is attained in water, the configuration of protein should also be qualitatively equivalent at a lower concentration. Such an apparent size distribution was considered to be in a state of non-equilibrium, temporarily produced by adding a physical force, e.g., ultracentrifugation, to the protein.

In particular, we obtained important information about the shape of UCH-L1 in water by SANS observation; namely, the wild-type UCH-L1 and the variants formed rotating ellipsoids. The possible existence of the ellipsoidal dimer was suggested previously by analysis of the sedimentation velocity [16], indicating that the sedimentation value corresponding to the dimer (4S) was smaller than that of twice the monomer (~2.3S). This discordance implied that the dimer was anisotropic, but not a sphere. Here, we noted the influence of a comparative change of the β-turn content by the substitution of amino acid to the protein structure, because as is well known, the β-turn content is an important component for constructing a three-dimensional structure, i.e., the globularity of protein [33,34] despite the low content. The relationship between the relative change of globularity (circular ratio = a/b, see SANS data analysis) and that of β-turn content is summarized in Table 1. Based on the wild-type, I93M substitution decreases the circular ratio to 58% and the β-tune content to 76%, whereas S18Y substitution increased the circular ratio to 179% and the β-tune content to 118%. If the S18Y substitution occurs on the I93M mutant, the circular ratio increases to 193% and the β-turn also increases to 156%. Conversely, the circular ratio decreases to 52% and the β-turn also decreases to 64%, if an I93M substitution occurs on the S18Y polymorphism. An I93M mutation rendered the ellipsoidal dimer more stable because of a decrease of the α-helix [24], increase of the β-sheet, and decrease of the β-turn. Conversely, S18Y substitution regained the globu-

Table 1
Relation between the relative change of ellipsoidal and β-turn by amino acid substitution

Type	Amino acid substitution	Circular ratio	Relative change of ellipsoidal	β-turn content (%)	Relative change of β-turn
Wild	Non	1.8*	—	6.6	—
	I93M	3.1*	0.58[a]	5.0	0.76[d]
	S18Y	1.0*	1.79[a]	7.8	1.18[d]
I93M mutant	S18Y	1.6*	1.93[b]	5.8	1.56[e]
S18Y polymorphism	I93M	1.6*	0.52[c]	5.8	0.64[f]

[a] The relative changes of the circular ratio of I93M and S18Y were calculated based on the wild-type, [b]based on the I93M, and [c]based on the S18Y.
[d] The relative changes of the β-turn content of I93M and S18Y were calculated based on the wild-type, [e]based on the I93M, and [f]based on the S18Y.
* The relative change of the circular ratio (a/b) was calculated.

larity of the dimer, and resulted in changing the ellipsoidal form of wild-type up to spherical, and also the ellipsoidal form of the I93M mutant up to a similar circular ratio of wild-type. The globularity of UCH-L1 variants is closely related to the variation of the secondary structures, further, to the locations of the substitution of amino acids on the protein. The location of residue 93 is near the hydrolytic active site and the substitution may directly restructure the local geometric configuration and affect hydrolytic activity. On the other hand, although the location of residue 18 is distal from the active site, the position is on the hydrophilic surface of the protein and the substitution may often affect β-turn formation (Fig. 1C). When two protein molecules form a spherical dimer by a very weak attractive force, such as the S18Y polymorphism, the presence of this type of oligomer cannot be detected by other methods except by SANS. Thus, that the globularity of the UCH-L1 molecule depends on the β-turn content was responsible for not only the dimeric configuration, but also the risk of Parkinson's disease.

Finally, we considered the relationship between configuration of wild-type UCH-L1 and UCH-L1 variants and their functions, i.e., multiple enzymatic activities, C-terminal hydrolase, and ubiquityl ligase (Fig. 6) [15,16,19–24]. The progressive deformation of the ellipsoidal form by the I93M mutation simultaneously impaired both the hydrolytic and ubiquityl ligase activities. This configurational defect could cause impairment of dynamic flexibility, which is necessary for enzymatic functions by the enlargement of the hydrophobic region. We can surely imagine the relation between progressive deformation of ellipsoidal dimer caused by I93M mutation and impairment of enzymatic functions. The restoration of globularity of monomeric UCH-L1 by S18Y substitution augmented the hydrolytic activity. In contrast, it markedly decreased the ubiquityl ligase activity. However, it is not easy to imagine why the restoration of globularity by S18Y substitution simultaneously decreases ubiquityl ligase activity and increases hydrolytic activity. Hydrolysis may be the dominant activity of UCH-L1, but it seems to be very sensitive to the dimeric configuration. However, the ubiquityl ligase activity may vary, coupled with the hydrolytic one, if both active centers are adjoined. However, the increased hydrolase activity of the S18Y coupled with its decreased ligase

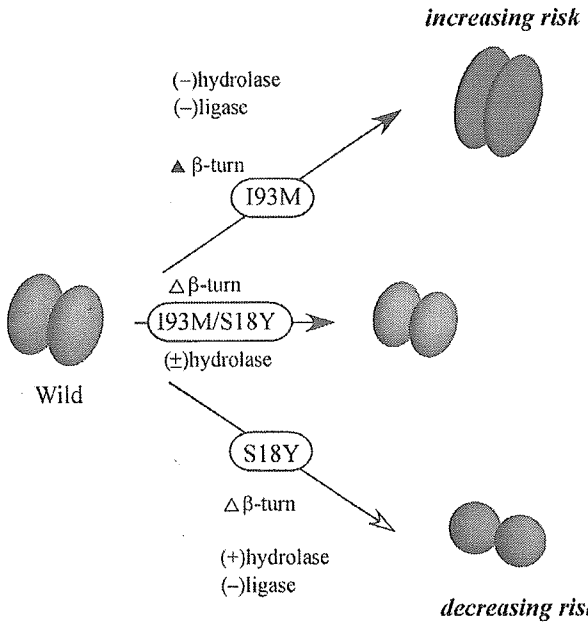

Fig. 6. Schematic speculative models of the relationship between the configuration of UCH-L1s in water and the multi-enzymatic activities. The self-assembled rotating ellipsoid wild-type dimer in water has both ubiquitin hydrolase activity and a ubiquityl ligase one. Both ubiquitin hydrolase and ubiquityl ligase activities decrease, as the result of an I93M mutation promoting the ellipsoidal deformation by a decrease of the β-turn and. A S18Y substitution recovers the globularity by an increase of the β-turn, causing an increase of ubiquitin hydrolase activity and a decrease of the ubiquityl ligase one. Thus, the variation of UCH-L1 hydrolytic activity caused by the deformation of the globularity of monomer component correlates to the PD risk.

activity (which can prevent α-synuclein degradation by K63-linked ubiquitin ligation) may be additive or synergistic with respect to the decreased risk of sporadic PD [16]. In this study, SANS observation may help in the confirmation of these hypotheses by observing either the hydrolytic digestion of ubiquitinated-proteins or oligomerization of free-ubiquitin based on the multiple enzymatic functions of PD-associated UCH-L1 variants. We demonstrated that SANS is an important technique for the direct observation of pathological protein assembly in water. We anticipate the design of a new SANS in the near future that is suitable for medical science and pathological analysis.